Journal of Civil Structural Health Monitoring (2025) 15:2059–2084
https://doi.org/10.1007/s13349-025-00927-9

ORIGINAL PAPER

Framework for a practical and cost-effective IoT-enhanced structural health monitoring and damage diagnostics system with digital twinning

Jack Huang[1] · André Broekman[1] · George Markou[1,2] · Hua-Peng Chen[3]

Received: 3 November 2024 / Accepted: 10 February 2025 / Published online: 10 March 2025

Abstract
Structural Health Monitoring (SHM) has emerged as a viable alternative to traditional visual and non-destructive assessment methods for civil infrastructure. The integration of sensor systems, the Internet of Things (IoT), and advanced data processing has further digitised SHM, leading to the development of Digital Twin (DT) technology, enabling dynamic, real-time simulations for proactive risk prediction and asset management. However, many existing DT-based SHM systems are costly, complex, and resource-intensive, limiting their practicality for small-scale implementations. This study investigates the feasibility of a practical and cost-effective SHM framework enhanced by DT technology for civil infrastructure. The hardware system explored two low-cost displacement sensors: a potentiometer contact sensor and an infrared non-contact sensor. During the static load testing, the potentiometer demonstrated high accuracy and stability, whilst the infrared sensor, despite higher noise, was effective for submillimetre measurements. These sensors were integrated with an IoT-enabled Arduino Nano 33 microcontroller for remote access via the cloud platform. The software system, "ReConTwin", developed using open-source resources, provides near real-time updates, analysis, and damage diagnosis through an automated post-processing system. The calibrated DT replicated the force–displacement response, accurately estimated the applied load, and closely predicted mid-span strain and crack formations of a Reinforced Concrete (RC) beam specimen subjected to short-term static three-point bending loads in a controlled laboratory setting. The user-friendly design and compatibility with standard commercial computers enhance the accessibility and feasibility of the proposed DT-SHM framework, making it a promising scalable solution for widespread adoption in real-world civil infrastructure applications.

Keywords Structural health monitoring · Digital twin · IoT · Sensors · Low-cost alternative · Damage diagnostics

1 Introduction

Railway and civil infrastructure are vital components of a nation's transport system, facilitating passenger and freight transit between major cities and ports. Despite continuous maintenance efforts, these infrastructures are rapidly ageing and deteriorating, diminishing their efficacy and negatively impacting commercial operations and global economic competitiveness. With rising traffic volumes to meet increasing transportation demands, maintaining existing infrastructure through conditional assessments and proactive maintenance is essential.

Currently, the industry primarily relies on visual inspections to assess the structural condition of civil infrastructure. Whilst these inspections provide a general overview and assist in identifying visible distress, they have significant limitations in accurately detecting structural concerns

✉ Jack Huang
jackhuang0824@hotmail.com

André Broekman
andre@broekmail.com

George Markou
george.markou@up.ac.za; george.markou@cut.ac.cy

Hua-Peng Chen
hp.chen@ecjtu.edu.cn

[1] Department of Civil Engineering, University of Pretoria, Pretoria, South Africa

[2] Department of Civil Engineering and Geomatics, Cyprus University of Technology, 3036 Limassol, Cyprus

[3] School of Transportation Engineering, East China Jiaotong University, Nanchang 330013, Jiangxi, China

and defects. Visual inspections are often subjective and inconsistent, with outcomes varying based on the inspectors' experience and the guidelines utilised [1]. In addition, visual inspections offer only discrete observations at a single point in time, being unable to detect subsurface and internal issues [2]. Other non-destructive testing methods, such as ultrasonic, radiography, and magnetic particle testing, are available but are inherently costly, labour-intensive, complex, disruptive, and potentially hazardous during their operation [3–5]. These challenges underscore the need for innovative, efficient, and timely monitoring approaches to ensure infrastructure integrity.

The Fourth Industrial Revolution has introduced innovative, data-driven smart technologies and solutions that are transforming traditional approaches to infrastructure management. Structural Health Monitoring (SHM) offers a promising alternative that addresses the limitations of conventional methods by providing continuous monitoring and evaluation of structural conditions. The integration of sensor systems, the Internet of Things (IoT), and advanced data processing has further enhanced SHM), leading to the novel concept of Digital Twin (DT) technology. A DT creates a virtual counterpart of a physical asset or system, enabling real-time monitoring, analysis, and predictive maintenance through prognostic processes [6]. Whilst sharing many similarities with conventional SHM systems, DT-based SHM offers several additional advancements:

- Enables automated, networked transmission, and real-time storage of sensor data, eliminating the need for manual transmission;
- Provides graphical information via IoT platforms (such as Building Information Modeling or cloud services) that can be readily accessed by end-users;
- Allows seamless integration of sensor data to modify analysis models, such as Finite Element (FE) models in a timely manner to predict the structure's realistic performance and conditions;
- Facilitates automated damage prognosis based on structural performance and suggests remedial measures.

DT-based SHM accentuates the digitisation and automation of the conventional SHM technique, promoting an intelligent, interactive, and proactive asset management strategy [7]. Mahmmodian *et al*. [8] describe that a complete DT system is characterised by the automation of information synchronisation between physical and digital assets. In the context of SHM for civil infrastructure, the digital entity receives real-time sensor data to dynamically replicate the physical structure's characteristics and predict its mechanical behaviour and response. Based on prognostic assessments, the DT provides automated preventive maintenance recommendations for asset managers to implement on the physical structure.

Several recent studies (since 2019) have showcased the use of IoT for real-time SHM in practical infrastructure projects. Armijo & Zamora-Sánchez [9] presented a case study on railway bridge monitoring using IoT sensors integrated with DT, demonstrating the effectiveness of real-time cloud storage, processing and machine learning for proactive maintenance. Bhatta & Dang [10] highlights how IoT technologies enhance SHM by enabling real-time data collection, improving decision-making, and automating maintenance process for civil engineering structures. It emphasises the benefits of IoT integration such as improved safety, reduced inspection costs, and extended infrastructure lifespan. Chang & Lin [11] demonstrated a real-time cloud-based monitoring system that uses IoT technologies and client-side web tools to process and visualise structural behaviours, such as displacement and acceleration, for active control and damage warnings. Di Nuzzo et al. [12] further expanded on this concept by utilising narrowband IoT (NB-IoT) technology and S (MEMS) accelerometers sensors to enable long-term, long-range, and low-power connectivity for the continuous monitoring of civil infrastructure.

Over the last decade, numerous research studies have explored the integration of DT technology with SHM systems for damage detection in infrastructure. Ritto & Rochinha [13] developed a DT framework by integrating physics based computational models with machine learning capabilities. The machine learning classifier serves as the DT, trained with a stochastic computational model to support real-time detection of structural damages. Shim et al. [14] proposed a DT-enhanced maintenance system for prestressed concrete bridges. This system combines a 3D DT model with a digital inspection system using image processing technology to identify and locate structural damage throughout the structure's lifecycle. Yu et al. [15] employed a DT-based hybrid SHM and fatigue evaluation method for the steel deck of a cable stayed bridge. This method synthesises monitoring data and FE models to develop a DT of a cable stayed bridge, enabling the prediction of fatigue cracking in the steel deck. Kong [16] explored DT applications for historic structures, demonstrating how photogrammetry-driven models can aid in preserving cultural heritage.

Despite its potential, the current landscape of DT-based SHM systems is faced with several challenges, including the high cost associated with advanced software and hardware components [17]. Implementing DT in civil infrastructure can be technically complex, particularly those adopting advanced features like machine learning and 3D image processing. It is crucial to design sensors with reduced power consumption and weight, as highlighted by Chacón et al. [18], to improve deployment and operational efficiency. In addition, the lack

of interpretability in some DTs may reduce user comprehension and confidence in prediction and diagnostic results, particularly when results are generated by complex algorithms or black-box models. Moreover, whilst comprehensive data collection is vital, it is essential to avoid over-measuring the physical model, focussing instead on outputs relevant for identifying potential damage and predicting future performance. Addressing these challenges is essential to making DT-based SHM systems more accessible and practical for widespread adoption in real-world civil infrastructure applications.

This research aims to develop a practical and cost-effective SHM framework enhanced by DT technology for civil infrastructure health monitoring. This study integrates low-cost displacement sensor technologies with IoT-enabled microcontrollers and develops a simple yet effective software system for real-time monitoring, analysis, and damage diagnostics. This study evaluates two displacement sensors, a potentiometer contact sensor, and an Infrared (IR) non-contact sensor, neither of which have been traditionally considered mechanical response measurement tools in past SHM systems. Both sensors are integrated with an affordable Arduino Nano 33 microcontroller to allow cloud-based data transfer. The developed software, named "ReConTwin", is developed using open-source resources to provide automated real-time updates, near real-time analysis, and damage diagnosis. The developed DT-SHM framework was tested on a Reinforced Concrete (RC) beam specimen under controlled laboratory conditions to replicate mechanical responses.

The significance of this study lies in demonstrating a feasible, accessible approach to SHM, particularly for contexts where traditional systems are cost-prohibitive or technically complex. The framework's emphasis on low-cost, user-friendly solutions highlights DT technology's potential to improve infrastructure monitoring and support proactive, data-driven asset management decisions. Whilst the study's feasibility is demonstrated in a controlled laboratory setting, its underlying principles are versatile and can be adapted and implemented for real-scale structures, making this approach a promising solution for future infrastructure maintenance and management.

The subsequent sections detail the development of the proposed DT-SHM framework for digitally twinning the mechanical behaviour of a monitored RC beam. Experimental results from bending tests of RC-beam specimens and the calibration of the DT FE model are presented. The evaluation focuses on the calibrated DT's reliability, sensor accuracy, and overall framework performance, assessed through mechanical response estimation, and damage diagnosis criteria.

2 Proposed DT-based SHM framework with damage diagnostics

2.1 Framework architecture

The primary objective of this research is to demonstrate the feasibility of establishing a practical and cost-effective SHM framework enhanced by DT technology for monitoring the health of civil infrastructure. The implementation focuses on the incorporation of the following key features:

- Affordable sensors;
- Real-time monitoring facilitated by a cost-effective wireless communication network;
- Relatively simple post-processing procedures;
- Interactive and user-friendly software interface.

In this research, a DT-based SHM system was developed to digitally predict the mechanical behaviour of a RC beam. The framework comprises two core systems, the hardware and software systems, which permit the automated transfer of data between the physical structural model and the virtual digital model in realising the smart monitoring of structural behaviour using DT principles (Fig. 1).

The hardware system is a smart sensor prototype that includes both the proposed contact and non-contact displacement sensors, as well as a cost-effective IoT-enhanced wireless communication sensor, capable of wirelessly transmitting real-time deflection data of the physical beam specimen to cloud storage. The software system constitutes a FE model-based, numerical model with automated and interactive post-processing functionalities, facilitated by a developed software programme named "ReConTwin". Its name was derived from the FE analysis software, *ReConAn FEA* (an abbreviation for Reinforced Concrete Analysis Finite Element Analysis), which ReConTwin uses to create the DT. ReConTwin extends *ReConAn FEA*'s capabilities, enabling it to digitally twin the RC-beam behaviour it analyses. Supported by ReConTwin, the software system was enabled to perform near real-time model updates for automated structural analysis, mechanical behaviour prediction, and damage diagnosis. These two core systems form vital links between the physical and digital object domains, permitting synchronised, automated data flow between the models.

2.2 Physical model and experimental setup

The physical model used to verify the proposed DT-based SHM framework in this experimental study consisted of a

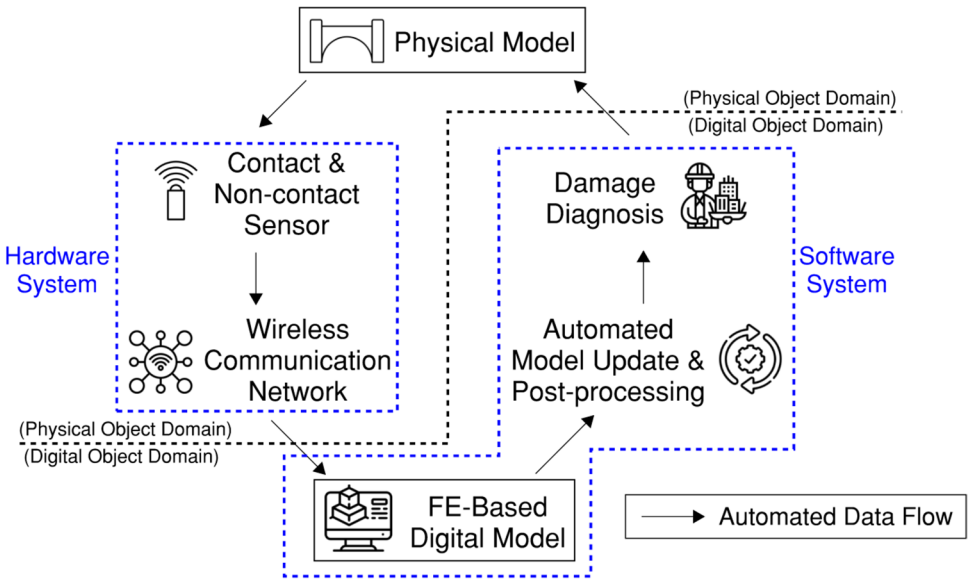

Fig. 1 DT-Based SHM framework architecture overview

RC-beam specimen constructed in a laboratory. Five identical RC-beam specimens were constructed, each measuring 2060 mm in length with a rectangular cross-section of 150 mm in width and 230 mm in depth. The beams were reinforced with two Ø12 mm bottom and two Ø10 mm top high-yield tensile longitudinal bars, with a nominal yield stress of 493 MPa, and Ø8 mm closed-loop mild steel stirrups spaced at 100-mm intervals along the beam length (Fig. 2 and Fig. 3). A 25-mm clear concrete cover was provided using plastic spacers. The concrete beams were cast with a mix using a water–cement ratio of 0.47.

The loading setup for all beam specimens involved a three-point bending configuration, with beams simply supported on roller supports over a clear span of 1800 mm. A vertical static load was applied at the mid-span using a contact roller connected to an MTS 500-kN hydraulic actuator. The load application was force-controlled at a constant rate of 4 kN per minute during both loading and unloading cycles. The beam specimens were tested in two stages:

- Load Test Stage 1: Four beam specimens were incrementally loaded to a maximum of 56 kN in 4 kN steps, with each load step maintained for 3 min. This stage aimed

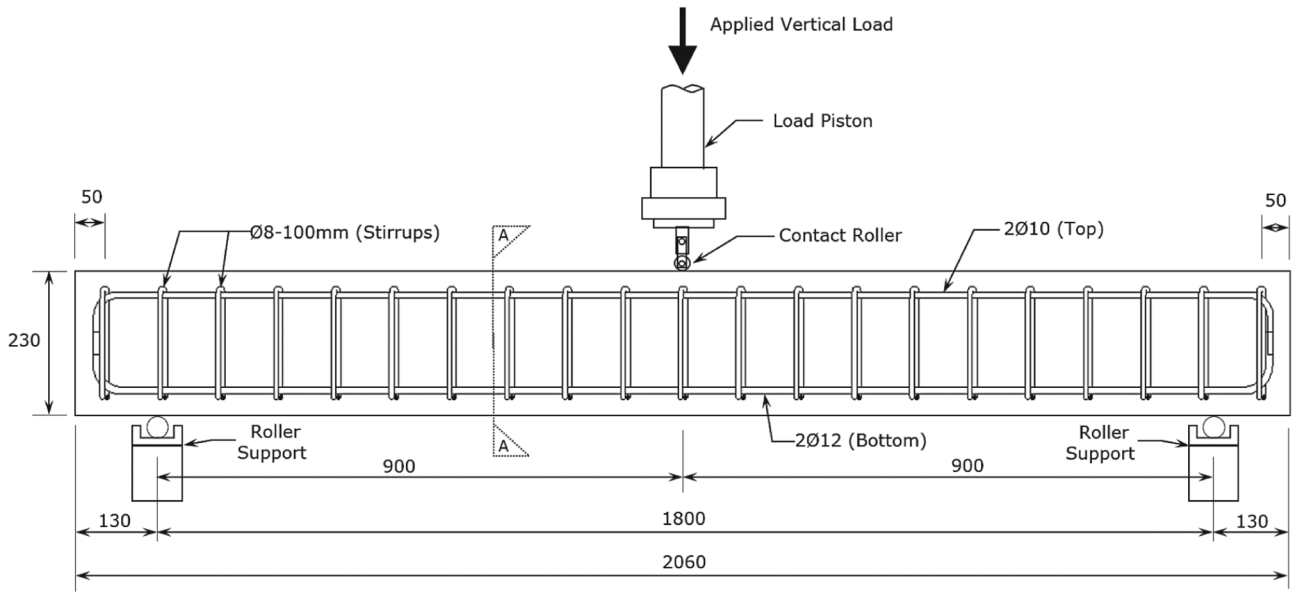

Fig. 2 RC-beam specimen elevation view (measurements in mm)

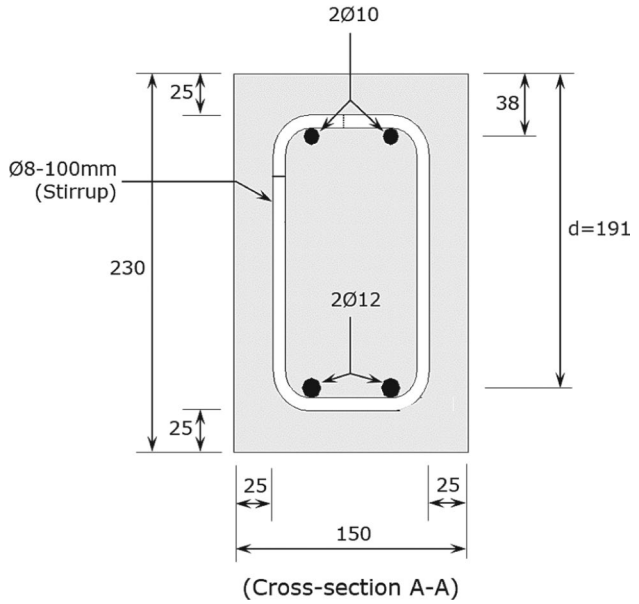

Fig. 3 RC-beam specimen cross-sectional view (measurements in mm)

to determine the average force–displacement response using a Linear Variable Differential Transformer (LVDT) sensor for vertical displacement measurement. Together with the known applied load, it served as benchmark data to calibrate the digital FE model. Surface strains measured by embedded Distributed Optical Fibre Sensor (DOFS) cables were compared against strain estimates from the FE model.

- Load Test Stage 2: A single RC-beam specimen, identical to those in Test Stage 1, was tested in two phases, with each load step maintained for 2 min. This test stage evaluated the performance of the hardware system (IoT-enhanced smart sensors) and the software system's ability to estimate the imposed load and surface strain of the monitoring beam:
  - Phase 1: The beam underwent three load cycles, progressively loaded and unloaded between 0 and 4 kN, 4 kN and 12 kN, and 12 kN and 20 kN, remaining within the elastic limit. This phase aimed to simulate day-to-day normal usage of the RC beam within its elastic limit.
  - Phase 2: The beam was subjected to an incremental loading procedure similar to Stage 1, reaching a maximum of 56 kN in 4kN load steps. This phase aimed to simulate conditions under which the beam was overloaded, exceeding its elastic limit.

Two control measurement systems, LVDT and DOFS, were utilised during load testing to measure vertical displacement

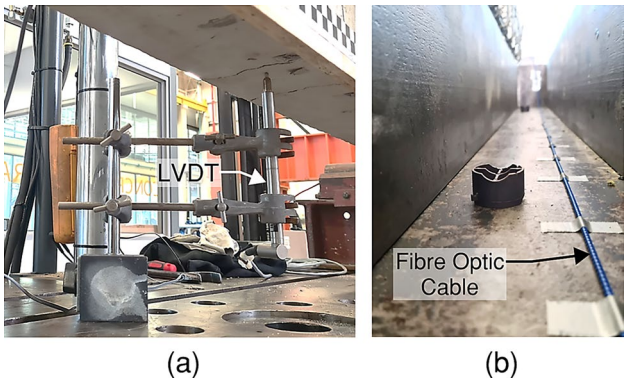

Fig. 4 Control measurement sensors: **a** LVDT and **b** FO cable along the beam cast mould bottom surface

and tensile strain at the beam's mid-span soffit, respectively. These sensors were not part of the proposed framework but were used to obtain control measurements for evaluating the proposed DT-based SHM framework. The LVDT, positioned centrally beneath the beam and supported by secured clamp arms to maintain contact with the beam's soffit (Fig. 4a), measured vertical displacement with a resolution of 1 µm. In Test Stage 1, the LVDT data and the applied load established a force–displacement benchmark for FE DT model calibration. In Test Stage 2, the LVDT assessed the accuracy of the proposed sensors.

The DOFS system, consisting of embedded Fibre Optic (FO) cables and a laser signal processing interrogator, measured maximum tensile strain along the beam's bottom surface, allowing multiple measurement points for maximum strain determination. Two types of FO cables were used: the 3.2-mm diameter BRUsens V9 cable by Solifos [19], encased in a metal tube with a polyamide sheath, provided flexibility, crush resistance, and high tensile strength, measuring up to 1% strain. This cable was straightened and attached to the beam mould surfaces with adhesive tape at a 120-mm interval before concrete casting (Fig. 4b). The second type was a 3-mm diameter E2000 cable by EFBElektronik [20], spliced to form a loop between the BRUsens V9 cables and the FO interrogator. Strain data were processed using the fTB 2505 interrogator by fibrisTerre [21], which operated using the patented Brillouin Optical Frequency Domain Analysis (BOFDA) technique to measure backscattered acoustic waves, achieving a spatial resolution of one reading every 52 mm.

3 Hardware system

3.1 Displacement sensors

Advances in sensor technology have enhanced performance whilst reducing costs, benefiting the development of

practical SHM systems. This research aims to demonstrate that affordable contact and non-contact sensors for measuring structural displacements can both provide precise results, making them ideal for DT-enhanced SHM frameworks. Two low-cost contact and non-contact sensors are proposed specifically for measuring the vertical displacement of monitored RC beams.

The contact sensor selected for this study (Fig. 5a) is a low-cost linear position sensor ($84 USD; €77 EURO) manufactured by Variohm EuroSensor [22]. The potentiometer operates as a passive transducer, measuring the potential difference in an electrical circuit relative to a known voltage. As a linear position sensor, the linear movement of an object causes the wiper to slide along the resistive track, adjusting the circuit's resistance and dividing the voltage proportionally. The sensor provides precise linear displacement measurements with a 50-mm maximum extension range, making it ideal for small-scale beam deflection measurements. Its electrical track is encased in a sealed membrane for compactness and minimal maintenance.

The non-contact sensor used in this research (Fig. 5b) is a low-cost IR light analogue distance sensor ($15 USD; €14 EURO) manufactured by Sharp [23]. It operates on the time-of-flight principle, emitting IR light pulses that reflect off surfaces and are detected by a photodiode receiver. By measuring the travel time of the light, the sensor accurately determines the distance. With a measurement range of 30 mm to 300 mm, the IR sensor is particularly well-suited for proximity sensing applications. Its affordability, fast response time, and reliable performance, even under varying reflectivity conditions, make it ideal for proximity and displacement measurements in this SHM application.

3.2 Wireless communication sensor

The Arduino Nano 33 IoT [24] (see Fig. 6) is a compact microcontroller equipped with wireless communication capabilities. Its compact size, affordability ($25 USD; €23 EURO), versatile Input/Output (I/O) pins, and wireless connectivity (Wi-Fi 802.11b/g/n 2.4 GHz and Bluetooth Low Energy 4.2) made it an ideal choice as a wireless communication sensor for seamless integration with the displacement sensors used in this research. The Arduino hardware is complemented by an open-source Integrated Development Environment (IDE) software platform, which provides an intuitive interface for programming and managing the

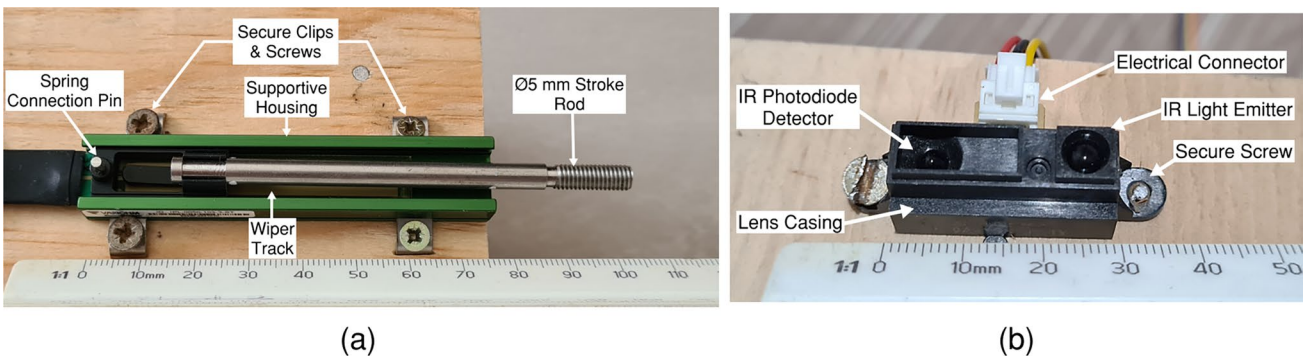

Fig. 5 Displacement sensors: **a** Linear potentiometer and **b** IR light distance sensor

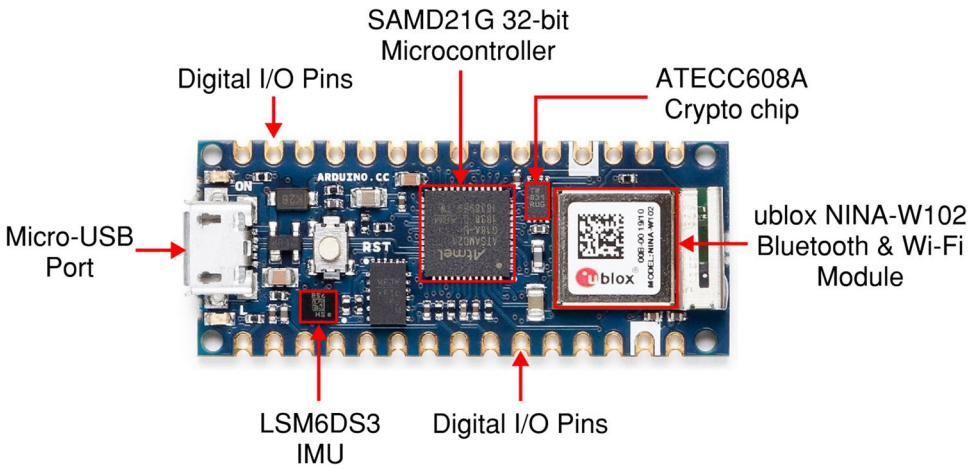

Fig. 6 Arduino Nano 33 IoT and key components [24]

microcontroller, making it easily adoptable even for individuals without advanced technical expertise. In addition, the Arduino IoT Cloud application supports the management of Arduino-based projects by offering tools for remote data visualisation, storage, and device management.

The Arduino microcontroller was programmed using an Arduino IDE sketch, which defined the measurement, calculation, and communication instructions. For each sensor, 250 samples were recorded and averaged to reduce noise, resulting in an average sampling time of 2.6 s per measurement for both sensors (0.39-Hz effective sampling frequency). This sampling rate was considered sufficient given the temporal nature of the progressive three-point bending static load test conducted within the framework of this study.

3.3 Hardware system assembly

The displacement sensors and the wireless communication microcontroller constitute the core hardware of the DT-based SHM framework with IoT capabilities. A schematic overview of the assembled proposed system, detailing its components and interconnectivity, is presented in Fig. 7.

During the experiment, the contact and non-contact displacement sensors were securely mounted on a support platform and elevated within their sensing range (see Fig. 8a). Positioned alongside the LVDT control sensor, they measured deflection at the mid-span location beneath the RC-beam specimen. The sensors were connected to the Arduino Nano 33 IoT microcontroller via digital I/O pins, utilising a compatible terminal adapter board to streamline wiring connecxions (Fig. 8b). The Arduino was housed in a 2-mm thick plastic enclosure. Due to the low-power consumption of the Arduino microcontroller and displacement sensors, both power and communication were supplied via a 5 V micro-USB cable connected to a laptop computer. The Arduino provided regulated 3.3 V for the sensors and digitised analogue displacement measurements from the RC beam using its internal Analog-to-Digital Converter (ADC). The laptop also served as a backup device, locally recording data during testing. The microcontroller's built-in Wi-Fi module enabled wireless connectivity with access points of mobile hotspots or conventional routers. This connexion allowed data transmission to the Arduino IoT Cloud, a free-to-use cloud-based platform for monitoring, controlling, and automating IoT devices. The real-time ADC data could be accessed remotely using a web browser or smartphone application, with encrypted data transfer ensuring secure communication.

3.4 Sensor calibration

Calibration was performed by comparing the sensor readings against a controlled displacement of a digital height gauge (Fig. 9). This procedure established the relationship between the analogue signals generated by the sensors and their corresponding digital outputs from the microcontroller's ADC. The calibration process was essential for defining the sensors' resolution, allowing for the direct conversion of ADC digits into meaningful displacement values. In addition, the calibration aimed to evaluate and quantify the sensors' accuracy, hysteresis, and noise characteristics.

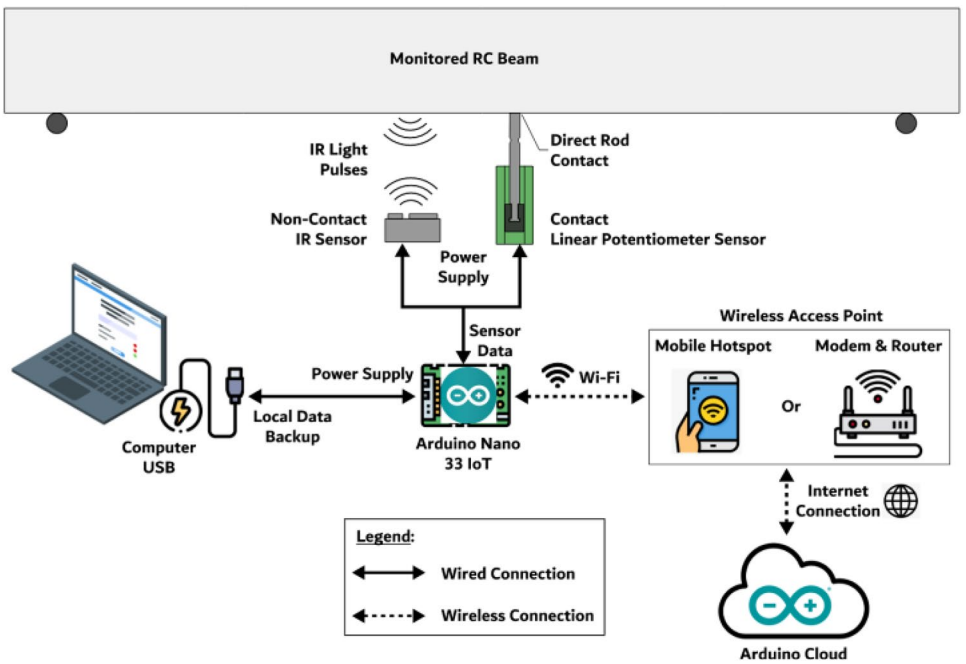

Fig. 7 Proposed hardware system overview

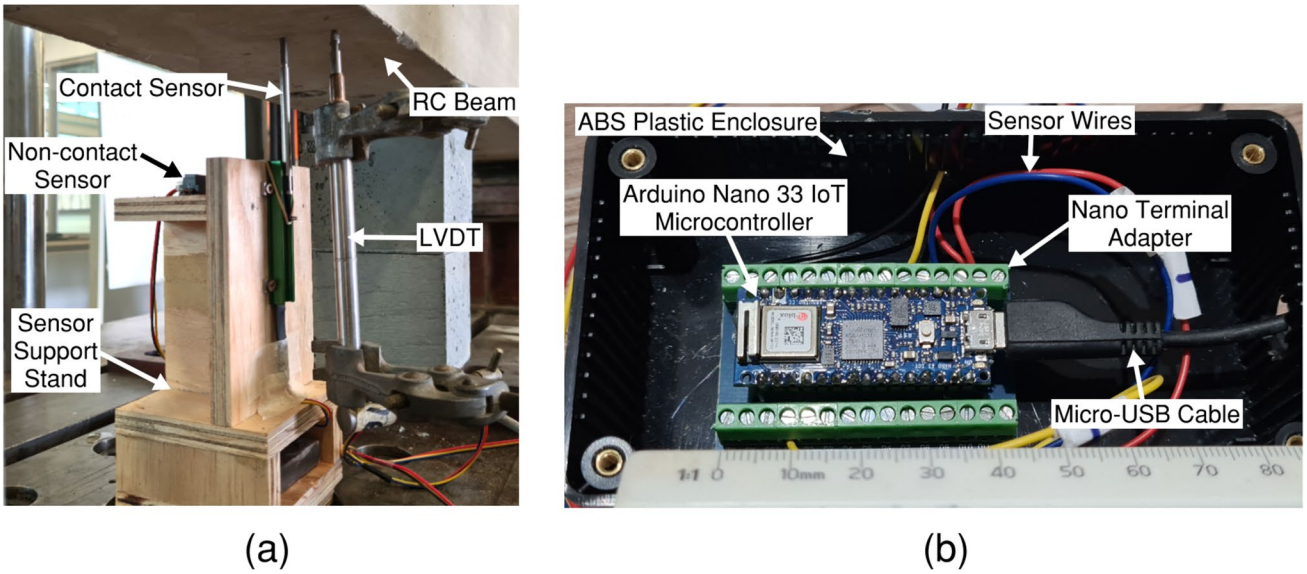

Fig. 8 Sensor assembly: **a** Displacement sensors and support platform and **b** Arduino microcontroller connection within the enclosure

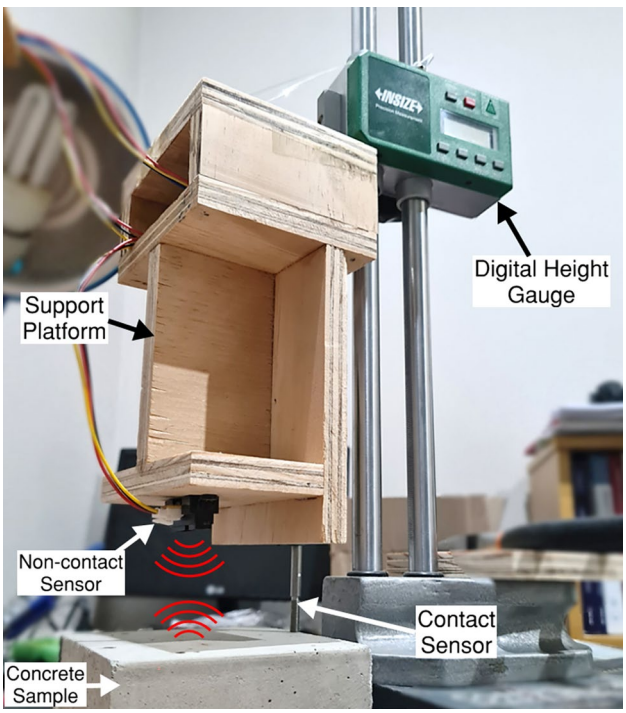

Fig. 9 Contact and non-contact displacement sensor calibration setup

The calibration results of the potentiometer contact sensor indicated a high degree of linearity between the applied displacement and ADC output, with a resolution of 48.4 µm per ADC digit. Conversely, the IR non-contact sensor exhibited a nonlinear relationship between detection distance and ADC output, represented by a quadratic polynomial function. This nonlinearity led to varying resolution, with higher resolution at closer ranges (94.1 µm per ADC digit at 32-mm detection distance) and lower resolution at greater distances (285.9 µm per ADC digit at 79 mm detection distance).

The accuracy of both contact and non-contact sensors was estimated by repeatedly sampling sensor displacements at four distinct reference measurement points using the height gauge through a series of increasing and decreasing distance cycles. By applying this approximated method, the accuracies were quantified to be ± 80 µm for the potentiometer sensor and ± 363 µm for the IR sensor (Table 1). The hysteresis was also calculated to be 0.11% relative to the total sampling extension length for the potentiometer (Table 2). Due to the highly complex and variable nature of the IR sensor's measurement, its hysteresis behaviour was not investigated in this study.

The operation of the sensor device can produce fluctuating ADC digit outputs, even when no physical changes are applied. This phenomenon is primarily due to electrical noise, including electromagnetic interference, voltage fluctuations, and thermal noise. This noise can influence the attainable measurement accuracy. To evaluate the noise characteristics of contact and non-contact sensors, a calibration test was conducted, sampling 1000 ADC digits at 0.39 Hz across various displacement points. In the calibration of the contact sensor, ADC digit samples were measured at three reference extension lengths of the potentiometer. Low standard deviations across all extensions indicate high precision and reliability in the measurements, producing highly consistent readings with minimal noise characteristics. In the assessment of the IR sensor, ADC digits were sampled under varying conditions, including different surface reflectivity, absorption, and lighting conditions.

Table 1 Accuracy calibration test data of potentiometer and IR sensors

Reading	Potentiometer sensor			IR sensor		
	Applied reference displacement [mm]	Measured displacement [mm]	Absolute difference [μm]	Applied reference displacement [mm]	Measured displacement [mm]	Absolute difference [μm]
First	15.210	15.256	46.0	15.870	16.431	560.7
Second		15.126	84.0		16.460	589.5
Third		15.178	32.0		16.488	618.4
First	25.210	25.229	19.3	25.870	26.194	324.1
Second		25.247	37.3		26.205	334.6
Third		25.145	64.8		26.184	313.7
First	35.210	35.109	101.0	35.870	36.391	521.2
Second		35.069	141.4		36.322	451.8
Third		35.165	44.6		36.423	553.2
First	45.210	45.067	143.1	45.870	45.916	45.7
Second		45.128	82.4		45.925	55.2
Third		45.078	132.5		45.973	102.7

Table 2 Hysteresis calibration test data of the potentiometer sensor

Load and unload cycle	Reference displacement [mm]	Maximum absolute measurement difference [μm]	Average absolute difference [μm]	Hysteresis (relative to total extension length) [%]	Average hysteresis [%]
1	25.388	39.623	34.697	0.13	0.12
	35.388	23.982		0.08	
	45.388	40.486		0.14	
2	25.388	41.195	35.699	0.14	0.12
	35.388	23.049		0.08	
	45.388	42.854		0.14	
3	25.388	41.195	28.397	0.14	0.10
	35.388	12.204		0.04	
	45.388	31.791		0.11	

Measurements of a concrete surface with acrylic white paint showed lower noise due to higher reflectance, especially at closer distances. Conversely, matte black paint led to higher noise due to lower reflectivity and higher IR absorption, particularly at closer distances. Testing in a dark room showed reduced signal dispersion at longer detection distances due to minimal ambient light interference. Across all conditions, noise generally increased with greater object distances from the sensor.

The potentiometer outperformed the IR sensor in terms of precision, accuracy, and resistance to noise, making it highly suitable for accurate displacement measurements. The IR sensor, whilst less precise, provided reasonable measurements at closer distances but was more susceptible to inaccuracies due to noise and environmental factors. The calibration highlighted the potentiometer's consistency and reliability, whereas the IR sensor's performance was influenced significantly by external conditions.

4 Proposed software system

The software system, in conjunction with the hardware system, is integral to realising the DT-enhanced SHM framework proposed in this study. It creates a synchronised loop between the physical asset and the digitally twined model, utilising the retrieved sensor data to dynamically replicate the monitored beam's mechanical behaviour and perform structural analysis to predict its physical response. The post-processed data are then used for damage diagnosis, providing early warnings, and recommending preventive actions in an interactive and timely manner. This allows asset managers to make informed decisions and implement a proactive SHM strategy.

The proposed software system was developed to be adaptable, accessible, practical, and cost-effective for small-scale applications, with the following objectives:

- Relatively straightforward post-processing using model-based FE analysis, eliminating the need for complex setups and computing power, whilst not compromising accuracy;
- Ability to calibrate the DT model using empirical load test data;
- Interactive and user-friendly interface;
- Capability to generate damage diagnostic report.

The development of the software components necessary to meet these objectives is detailed in this section.

4.1 FE-based digital model

The DT of this study aimed to replicate the mid-span force–displacement mechanical response of a RC beam subjected to three-point bending using FE modelling. This was accomplished through a model-based approach that simulated the beam's geometry, material properties, boundary conditions, and applied loading. The baseline FE model, representing the preliminary, uncalibrated DT, was created using *FEMAP* [25], a simulation software designed for the pre- and post-processing of complex engineering models. *FEMAP* enabled the replication of key characteristics of the RC beam, including its geometry, concrete and steel properties, support conditions, and applied loading.

The baseline model data were exported as a *FEMAP* neutral file, readable as a text file, and compatible with *ReConAn FEA* [26]. After nonlinear analysis in *ReConAn FEA*, the built-in post-processing window, *ReConAn Eye*, was automatically initialised to visualise and animate 3D concrete beam cracking and deformation. The analysis results could also be re-imported back into *FEMAP* for further post-processing, including visualisations of model deformation and contour plots of solid von Mises stress and strain. Since *FEMAP* cannot directly illustrate cracks at FE nodal points, *ReConAn Eye* provided graphical representations of 3D cracks as they resulted from the numerical nonlinear analysis.

The structural analysis of the FE model was conducted using *ReConAn FEA* [26], a specialised RC FE analysis software renowned for handling advanced numerical methods and nonlinear material modelling. *ReConAn FEA*, developed with object-oriented programming, operates efficiently on standard commercial computers whilst delivering accurate RC structure simulations. Unlike software that requires specific file formats, the software reads FE model inputs and exports results in a universal text format, enhancing compatibility across multiple software platforms and operating systems. Its extended post-processing feature, *ReConAn Eye*, provides visualisation and animation of predicted concrete crack formations, offering further insight into the structural behaviour of the analysed RC members. Figure 10 illustrates the aforementioned FE-processing procedures, along with the related file types and software involved.

The concrete beam was modelled in *FEMAP* with 20-noded hexahedral FE solid elements, employing a smeared crack approach and an elasto-plastic material model based on the modified Kotsovos & Pavlovic model [27] as proposed by Markou & Papadrakakis [28] (see Fig. 11). The Kotsovos and Pavlovic model, introduced in 1995, is a three-dimensional constitutive material model designed to simulate the nonlinear behaviour of concrete under various loading conditions [29]. It effectively captures the complex stress–strain relationships characteristic of concrete, including phenomena such as micro- and macrocracking. Subsequent enhancements by researchers such as Markou and Papadrakakis [30] have refined the original model, enhancing its computational efficiency and accuracy. These modifications have significantly increased the model's effectiveness in simulating the behaviour of RC structures under both static and dynamic loading conditions [31]. Furthermore, the model has been successfully applied to simulate the cyclic behaviour of RC structural members, demonstrating strong agreement with experimental observations [32]. Overall, the modified Kotsovos and Pavlovic model provides a robust and reliable framework for modelling the nonlinear behaviour of concrete structures, with validation studies confirming its strong correlation with experimental data.

The reinforcing bars were represented as rod elements with bilinear steel behaviour [33]. Boundary conditions simulated a simply supported beam-test configuration, with support nodes constrained to prevent local failure. The loading was applied at the mid-span and distributed proportionally

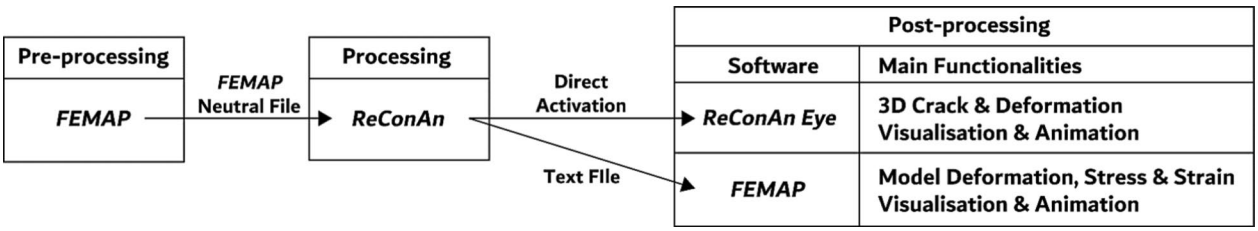

Fig. 10 FE-processing procedures, file type and software employed for the software system's DT

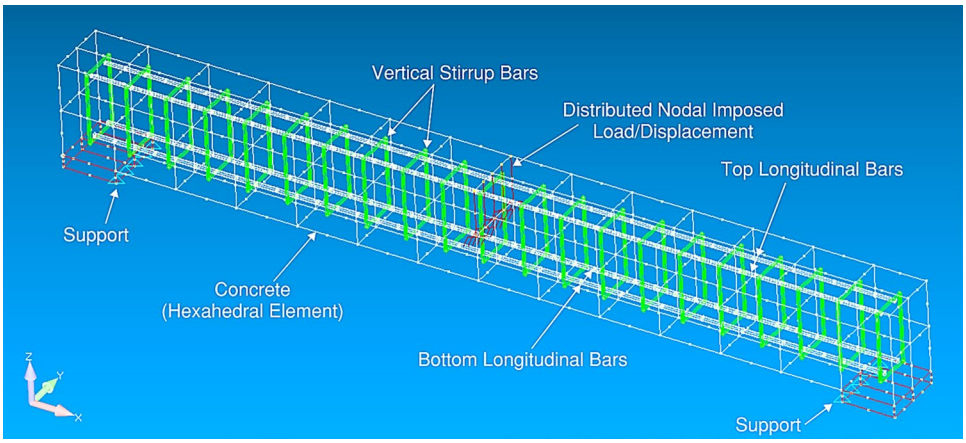

Fig. 11 FE baseline model developed in *FEMAP*

across five central nodes. The calibration process employed a displacement-controlled Newton–Raphson method over 50 load increments.

4.2 DT calibration process

Following the creation of the baseline FE model, calibration using load test results was essential to achieve a DT with higher accuracy in predicting the mid-span force–displacement behaviour of the experimental beam specimen. Calibration is widely regarded by numerous researchers as a critical procedure in validating and updating the FE model in a DT framework. For this study, the DT was calibrated using Load Test Stage 1 results (detailed in Sect. 2.2), allowing the baseline model to be iteratively refined to replicate the tested force–displacement response. Provided that the beam specimens in both load test stages shared identical geometric and material properties, the calibrated DT could be confidently utilised to predict the mechanical behaviour of the beam in Load Test Stage 2.

Discrepancies between the baseline FE model and the physical beam's behaviour were anticipated, largely due to material property variations, construction quality, and experimental setup differences. However, in the controlled laboratory environment, the primary factors influencing the force–displacement behaviour were identified as:

- Young's modulus of concrete;
- Young's modulus of reinforcing steel;
- Yield stress of reinforcing steel.

These material properties were selected as the key varying parameters in the iterative calibration process of the DT model. The calibration process involved the iterative analysis of the FE numerical model with all possible combinations of these three material properties (Fig. 12). The DT corresponds to the force–displacement response that most closely resembles the load test result.

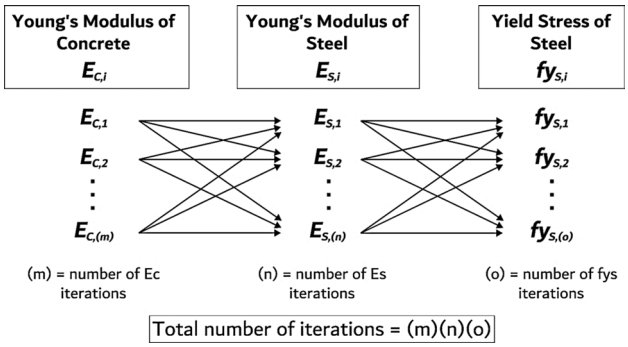

Fig. 12 Analysis iteration with variations of concrete and reinforcing steel material properties

This simplified approach enabled a realistic and reliable simulation of the RC beam's mechanical response. Whilst increasing the number of iterations would increase the probability of finding a similar iteration, it would also lengthen the analysis time. Therefore, the iteration ranges were carefully selected based on material test results and sound engineering judgement to balance accuracy and computational efficiency.

4.3 ReConTwin — automation and user-interface

To fully realise the automation and user-friendly interface capabilities of the DT-integrated SHM framework, the software application, ReConTwin was developed. ReConTwin serves as an indispensable component in optimising information flow and enhancing interactivity between the digital model and the asset management team. Visual Studio Code (VSC) [34], supports various programming languages, facilitating efficient code management, editing, and debugging processes.

Python, a versatile script-based, interpreted programming language, was central to automating ReConTwin's DT calibration process, reducing manual effort in repetitive tasks.

Python scripts were created for ReConTwin to automate each repetitive step of the iterative procedure:

- ReConTwin replaces the manual update process in *FEMAP* by directly modifying the material property parameters in the baseline FE model's neutral file.
- Subsequently, ReConTwin autonomously activates *ReConAn FEA* to perform a displacement-controlled FE analysis based on the updated neutral file. The desired imposed displacement can be selected by the user based on the recorded live displacement readings from the Arduino Cloud. Upon completion, *ReConAn FEA* exports the analysis results to a text file.
- In the next step, ReConTwin extracts the back-calculated vertical load and displacement increments, storing them as force–displacement entries in a Microsoft (MS) Excel result file. During this step, the relative error of each iteration is calculated and recorded. The aforementioned three processes are repeated until all iterations are complete.
- Finally, ReConTwin selects the iteration with the smallest error as the most accurate DT model that best simulates the mechanical response of the RC beam.

In addition to automation, ReConTwin was developed with Python-based scripts to create user-friendly interfaces, enhancing intuitive interaction with the software system. The Graphical User Interface (GUI) was built using Tkinter, a popular Python library, to visually and graphically display input and output data generated by the proposed SHM framework (Fig. 13).

Illustrated by Fig. 14, four interdependent GUI windows were developed, enabling the user to specify preferred input parameters, automate tasks, and navigate through ReConTwin using graphical elements such as input fields, buttons, and display plots [35]. These windows include:

- GUI Window 1 – Parameter input window. Allows users to input parameters for the DT calibration process, including material properties and deflection limits.

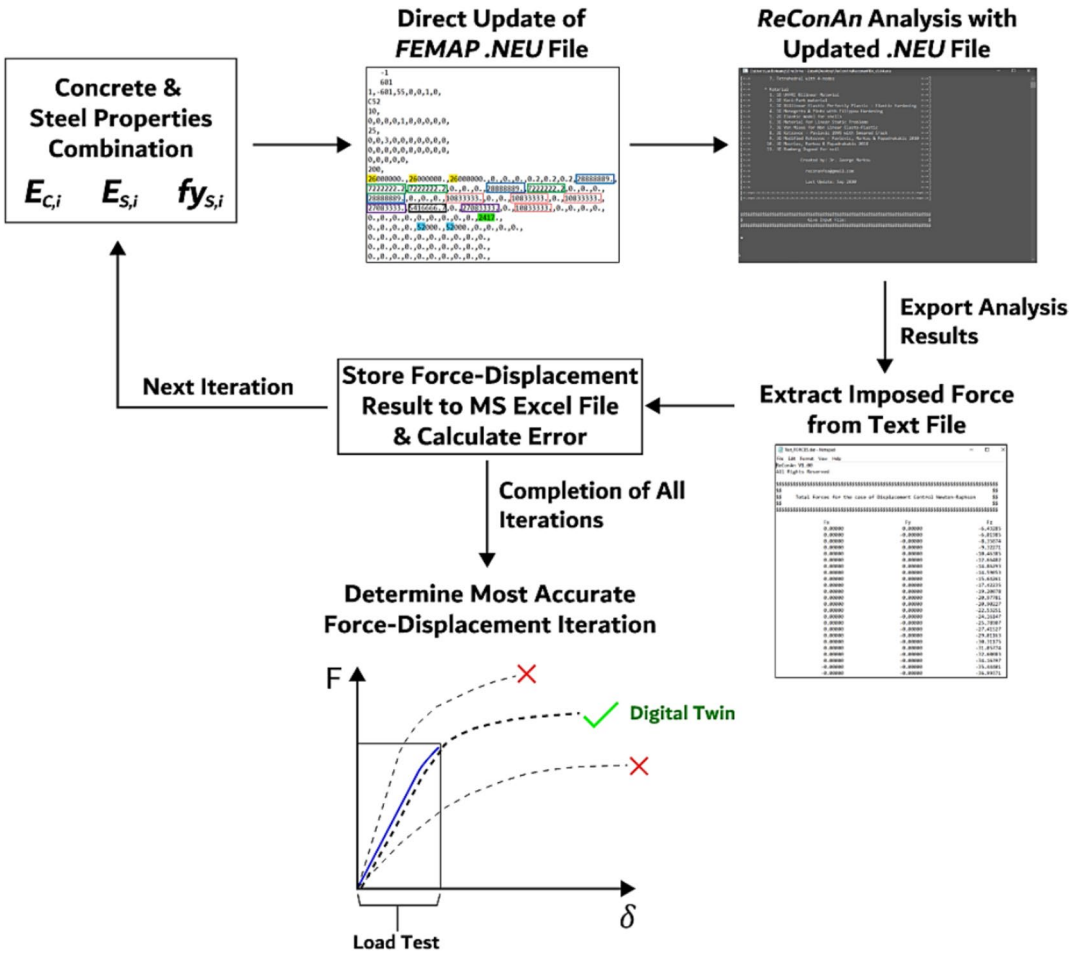

Fig. 13 ReConTwin's automated DT calibration process using the Python code

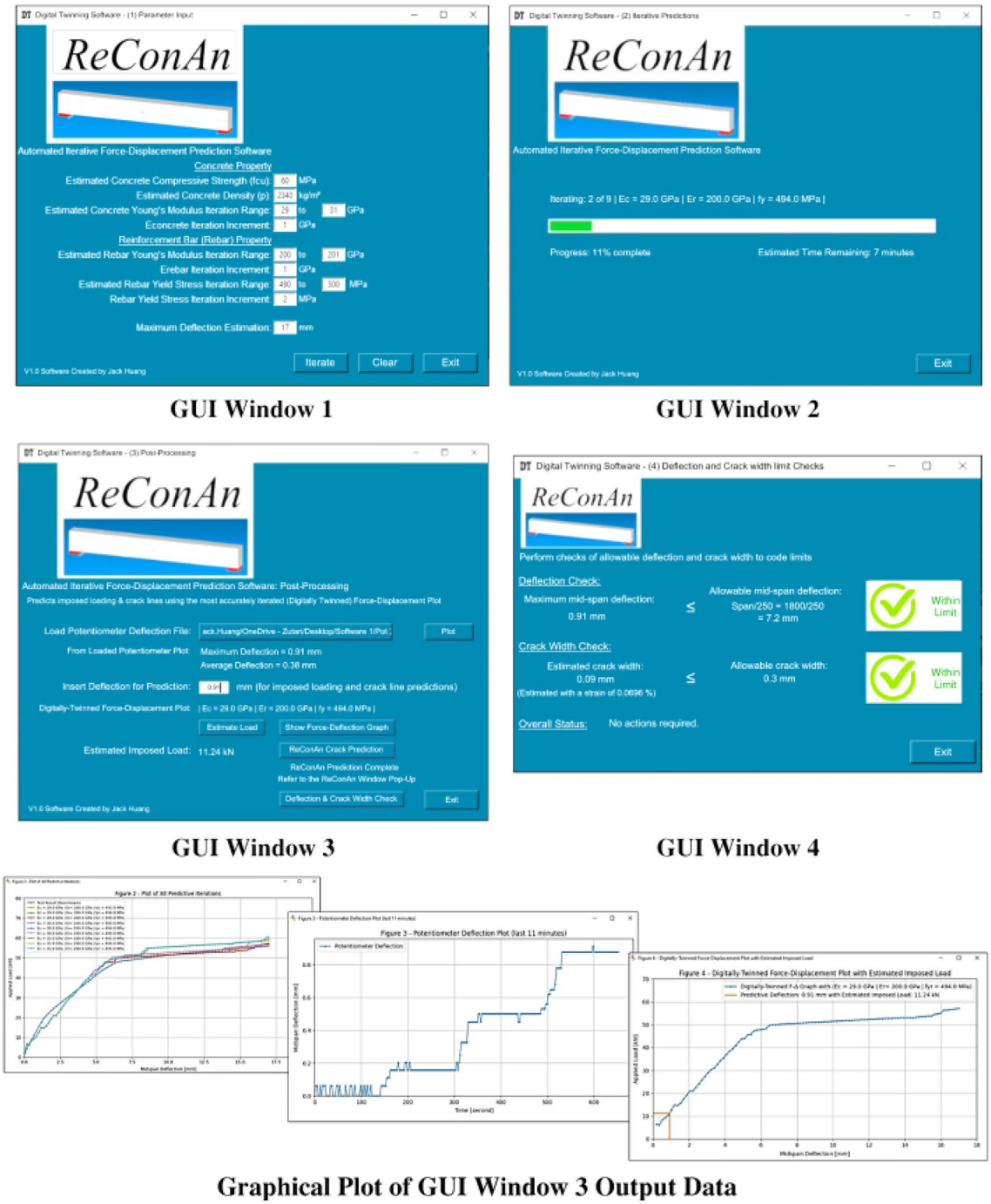

Fig. 14 GUI windows and graphical plot of data generated by ReConTwin

- GUI Window 2 – DT calibration window. Displays the calibration procedure progress and enables users to review prediction results and the most accurate material property iteration.
- GUI Window 3 – Post-processing window. Enables users to incorporate sensor data to predict force–displacement behaviour, plot sensor data, estimate imposed load, and predict crack formation.
- GUI Window 4 – Damage diagnosis window. Automates damage diagnosis based on performance indicators relating to beam deflection and crack width limits, providing preventive action alerts.

By integrating automation and user-friendly interfaces, ReConTwin streamlines processes, enhances efficiency,

and offers transparent, intuitive navigation, allowing users to holistically control the DT-SHM framework.

4.4 Damage diagnosis

The final stage in completing the automated information synchronisation between the DT model and its physical RC-beam counterpart involves ReConTwin's damage diagnosis functionality (GUI Window 4). This feature evaluates the structural condition of the monitored RC beam and provides an early warning to the user if performance is not within the expected criteria. Two key structural performance indicators are assessed:

- Mid-span deflection limit: ReConTwin verifies whether the mid-span deflection, based on imported sensor data in GUI Window 3, complies with the span-to-deflection ratio of 250 (or user-defined limit).
- Crack width limit: The estimated crack width, derived from the beam soffit strain using *ReConAn FEA* analysis, is compared to the limit of 0.3 mm (or user-defined limit).

If either limit is exceeded, ReConTwin will generate a warning, prompting preventive action. This automated process improves the identification of structural issues, enhancing the reliability and safety of the structure. *ReConAn FEA*'s integration with 3D modelling further enables comprehensive evaluation of the monitored RC structure, allowing users to anticipate not only superficial crack formation but also internal damage within the RC domain.

4.5 Software system overview

The overview of the developed software system, integrated with ReConTwin, forms a key part of the proposed DT-SHM framework. Its components, processes, and automated information flow outlined in in Sect. 4, are illustrated in Fig. 15.

Following the transmission of real-time beam displacement sensor data to the Arduino IoT Cloud from the hardware system (Fig. 7), the user can access this data from the cloud via a computer or smart device, and then import it into ReConTwin for analysis. ReConTwin uses this data to predict the vertical load imposed on the RC beam and assess crack width for damage diagnosis. The software system is equipped with the capability to calibrate the FE numerical model preliminarily or periodically, ensuring the generation of a reliable DT. The repetitive process in the iterative predictive analysis procedure is automated by ReConTwin, simulating the force–displacement behaviour based on the load test results with minimal human intervention. The resulting damage diagnostic report outlines the structural condition and performance of the RC beam, along with the estimated applied load and numerically predicted cracks. These results can then be examined by the asset management team to gain insights into the structural performance and condition of the beam, predict potential damages, and take preventive actions in maintaining the infrastructure asset, thereby fully realising the DT-enhanced SHM framework.

5 Experimental work and results

5.1 Load test stage 1 and DT calibration

In the first stage of the loading test, four RC-beam specimens underwent a three-point loading test as outlined in Sect. 2.2 (Fig. 16). An incremental static load of 4 kN was applied at a rate of 4 kN per min and maintained for 3 min at each load step until failure. The corresponding displacement for each load step was calculated as the averaged displacement from the load-maintaining phase.

Each specimen was tested to failure reaching the peak load of 52 kN. The force–displacement relationship for each beam and the calculated average, are shown in Fig. 17. The standard deviation of the mid-span displacements increased with higher loads, indicating a more consistent response at lower loads and greater variability at higher loads. The measured displacements of the RC-beam specimens under various applied point loads exhibit a consistent force–displacement behaviour, serving as reliable control data for calibrating the DT.

During each load-maintaining phase, the distributed FO interrogator recorded tensile strain along the beam's soffit, generating a progressive strain growth profile. A typical positive strain profile growth is illustrated in Fig. 18. Strain increased with applied load, but the location of maximum strain varied due to nonlinear cracking, material inconsistencies, and imperfections. The distributed optic fibre allowed the identification of the largest tensile strain for each beam at every applied load step. The averaged maximum strains for all beams were then used to compare with the strain predicted by the DT numerical model.

Using the average force–displacement results as a control benchmark, the FE numerical baseline model was calibrated to create a DT capable of accurately predicting the mechanical response of the RC beam in Load Test Stage 2. The calibration process involved iterative structural analyses to adjust the FE model's material properties to closely resemble the load–displacement experimental data. Two groups of input vectors were defined for this process: basic property and iterating material property. The basic property consists of non-varying properties that remained constant throughout all iterative FE analyses. Conversely, the iterating material property vector consists of three main material properties pertaining to concrete and reinforcing steel

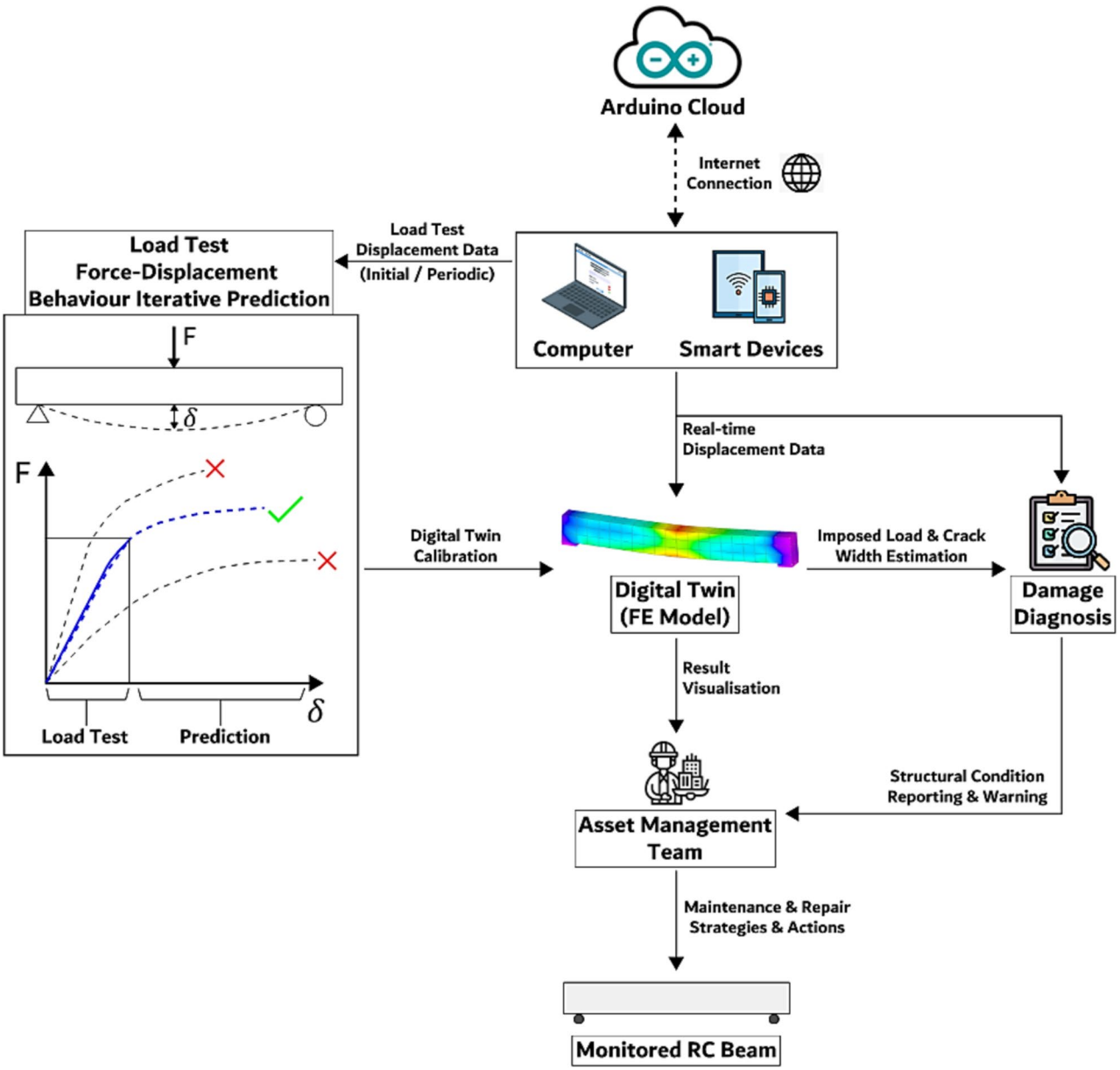

Fig. 15 Software system overview

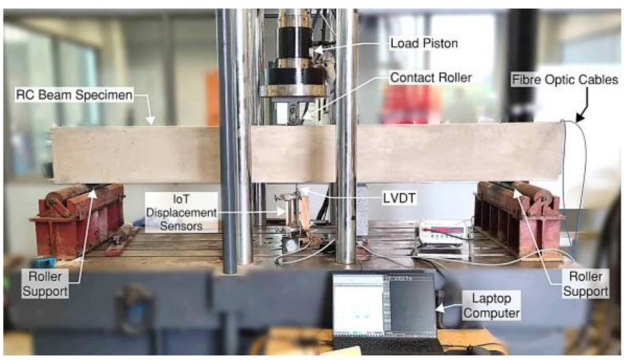

Fig. 16 Typical three-point bending test of RC-beam specimens

that varied during the iterative process. The basic properties included concrete compressive strength (56 MPa), concrete density (2378 kg/m^3), and maximum deflection (17 mm). The iterating properties involved concrete Young's modulus (ranges from 26 to 34 GPa with 1 GPa increments), reinforcing steel Young's modulus (200 GPa), and steel yield stress (493 MPa to 500 MPa with 1 MPa increments). These values were specified based on the concrete and reinforcing sample test result values and sound judgement.

The calibration process, automated through ReConTwin (Fig. 19), comprised a total of 72 nonlinear analysis iterations, combining the different material properties. Each iteration required approximately 50 s to complete, yielding

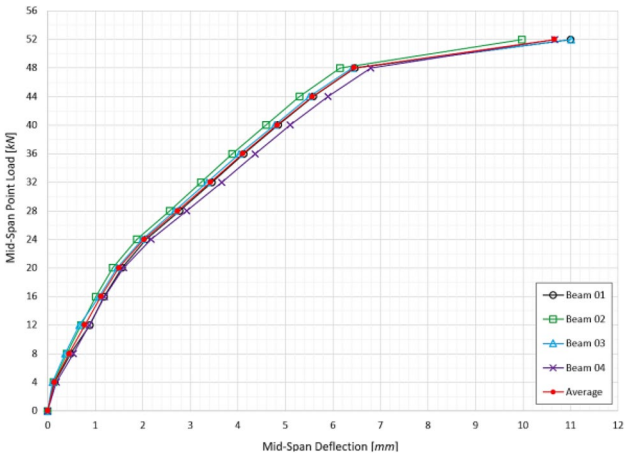

Fig. 17 Force–displacement results at beam mid-span (Load Test Stage 1)

a total calibration time of an hour. After each iterative analysis, the corresponding force–displacement results and calculated relative errors were recorded in the MS Excel workbook. This file was available for review at the end of the calibration procedure, enabling an evaluation of the calibration's accuracy and serving as a comprehensive record of the iterative process.

Upon completing the iterative FE analyses, ReCon-Twin identified the iteration with the smallest relative error compared to the load test control data. This iteration was then set as the DT model to accurately simulate the force–displacement response of the RC-beam specimens, and the calibration outcomes were updated in GUI Window 2 (Fig. 20).

GUI Window 2 also provided post-processing capabilities, allowing users to review the calibration results through force–displacement plots (Fig. 21). Based on the review of these plots, users could adjust input parameters in the first GUI window and reperform the DT calibration to achieve the desired accuracy. Out of 72 iterations, the DT with a mean relative error of 4.7% was identified. The material properties for this iteration were:

- Concrete Young's Modulus: 29 GPa;
- Reinforcing Steel Young's Modulus: 200 GPa;
- Reinforcing Steel Yield Stress: 494 MPa.

The force–displacement behaviour across the 72 iterations was consistent within the 0 kN to 50 kN load range. At lower loads, the iterations displayed lower bending stiffness than the control, but at higher loads, particularly beyond 34 kN, the stiffness increased, reflecting the strain-hardening effect of the reinforcing steel. The curves flattened as the steel reached its tensile yield strength of approximately 40 kN, closely mirroring the control data where yielding occurred around 48 kN. Beyond 50 kN, the iterations showed slight overestimations in stiffness, attributed to higher steel yield stresses in some iterations. These discrepancies were linked to factors such as strain hardening, cracking mechanisms, bond-slip characteristics, and creep, which contribute to

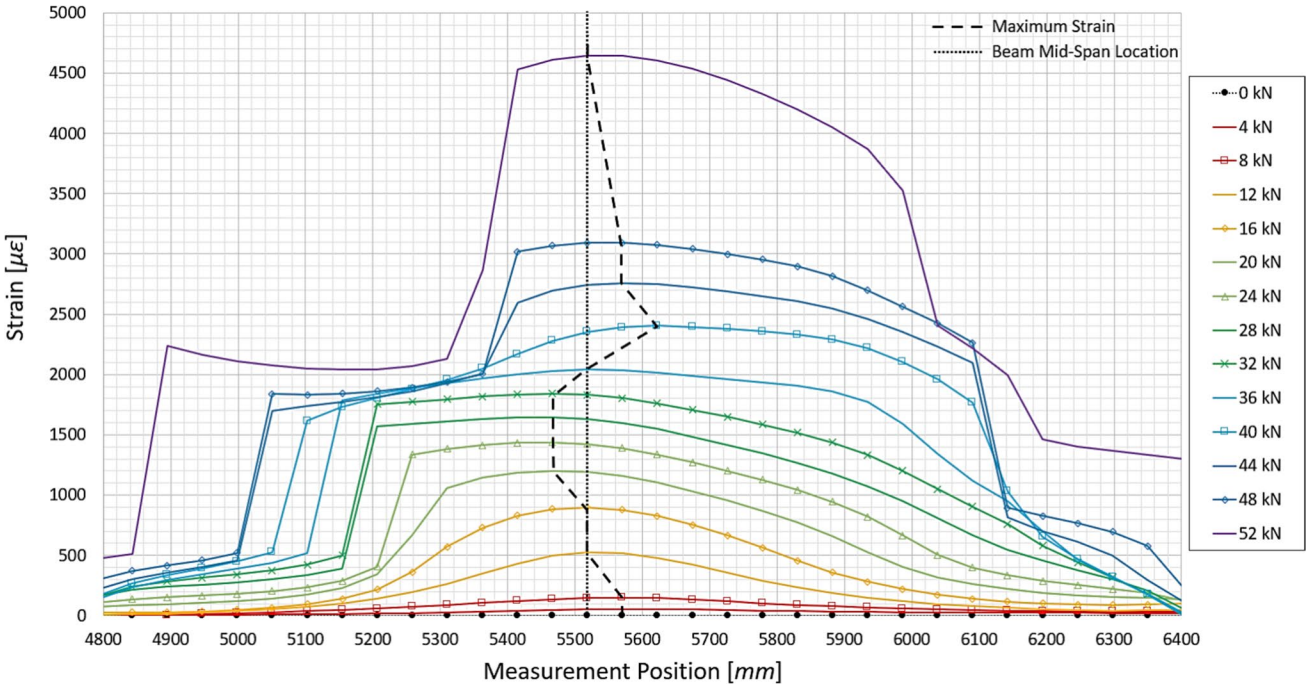

Fig. 18 Typical distributed optic fibre strain growth profile along the beam soffit (Load Test Stage 1)

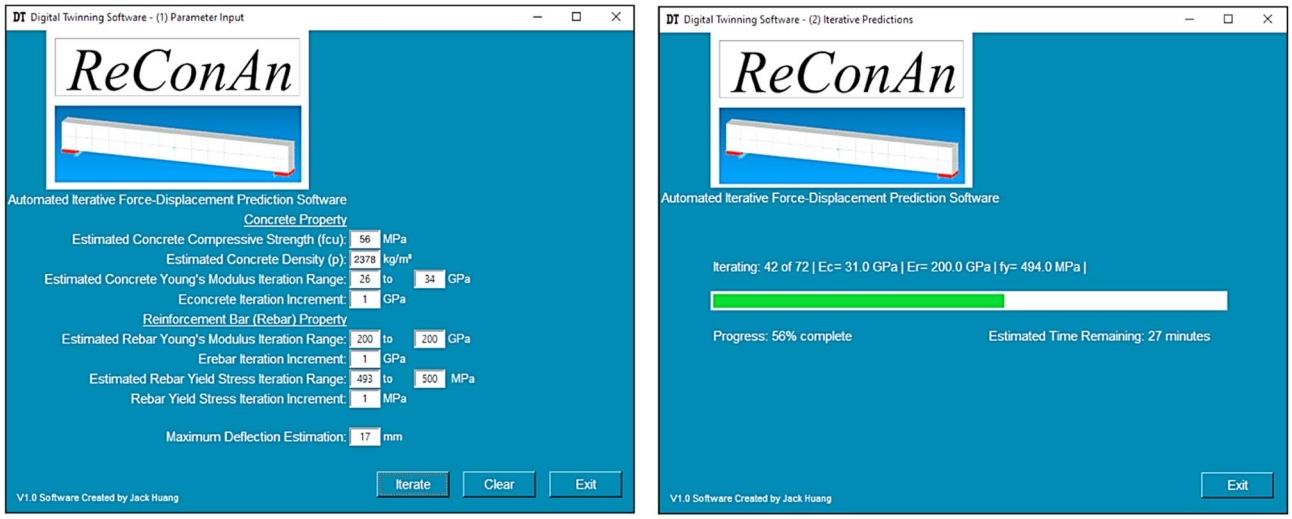

Fig. 19 ReConTwin: **a** GUI Window 1, calibration parameter input and **b** GUI Window 2, calibration progress display

Fig. 20 ReConTwin: GUI Window 2, calibration completion display and result review functionalities

inherent challenges in achieving perfect agreement between nonlinear FE models and experimental results. Despite these discrepancies, the most accurate iteration (Fig. 21b) closely aligned with the control data, with a relative error of 4.7%, demonstrating that the DT calibration effectively captured the mechanical response of the RC beam across the entire load spectrum.

The automated, iterative approach employed in this study effectively created a DT capable of accurately simulating the mechanical response of the RC-beam specimen. By utilising a relatively uncomplicated procedure that avoids the need for complex calibration processes or intricate FE models, and by making reasonable assumptions within this study's framework, this method has demonstrated to be a robust and efficient method to develop reliable DTs that can accurately predict the structural behaviour of the monitored structures.

5.2 Load test stage 2 and smart sensor performance

In the second load test stage, the final RC-beam specimen was subjected to two phases of three-point bending tests: static–cyclic and static–incremental loading. The developed IoT-enhanced smart displacement sensors were used to monitor the mechanical response of the beam under different loading conditions.

5.2.1 Phase 1 – static–cyclic load test

In the first phase of the load test, the RC-beam specimen underwent short-term, static–cyclic loading with three repetitive and progressive load cycles (0 kN to 4 kN, 4 kN to 12 kN, 12 kN to 20 kN) applied at the beam mid-span whilst remaining within the beam's elastic limit. The loading and unloading were carried out at a rate of a minute per load step, with each load step maintained for 2 min. The displacements of the overall static–cyclic test measured by the potentiometer, IR sensor, and the LVDT control at the beam soffit are shown in Fig. 22.

Mean displacements for each maintained load step were calculated by averaging all measured displacements during each maintaining period for all three sensors. In comparison to the LVDT, the Mean Absolute Error (MAE) values for the potentiometer remained consistently low (2.7 µm to 64.4 µm) with an overall average MAE of 25.2 µm.

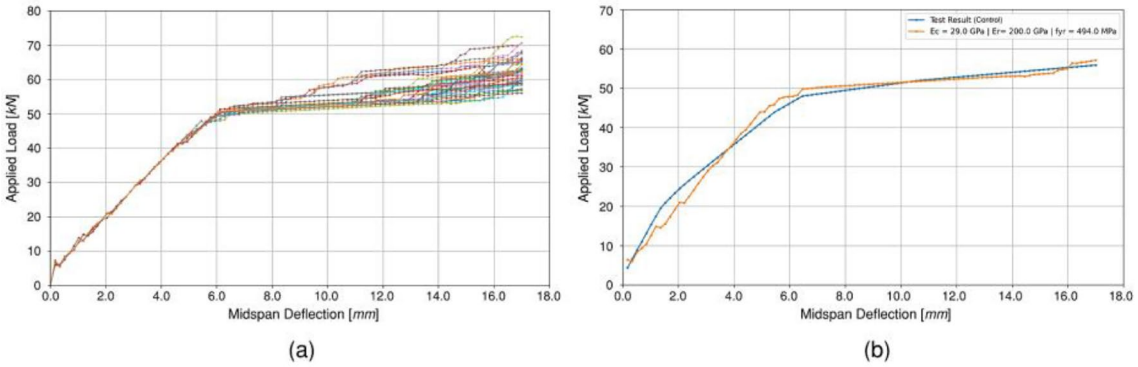

Fig. 21 ReConTwin, GUI Window 2, force–displacement result graphical plot: **a** All iterations with control result and **b** The most accurate iteration (DT) with control result

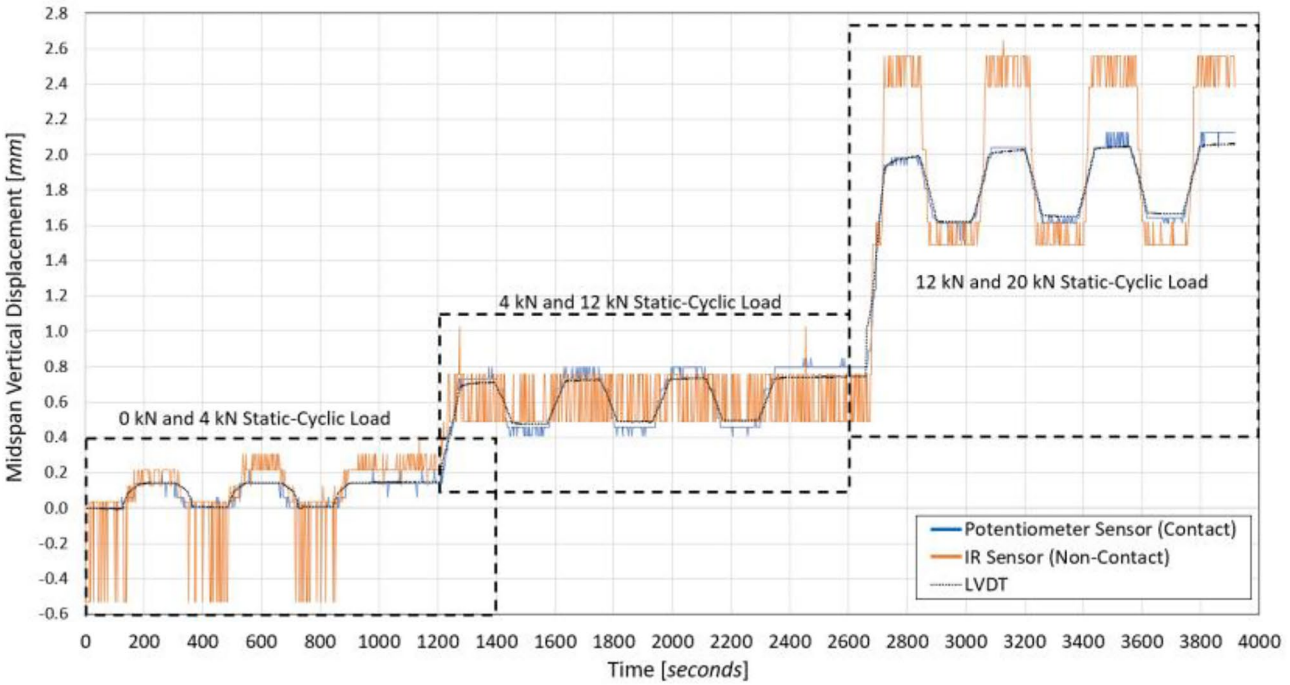

Fig. 22 Overall static–cyclic test displacement results (Load Test Stage 2, Phase 1)

Conversely, the IR sensor showed significantly higher errors (48.8 µm to 500.2 µm) with an average MAE of 184.8 µm, particularly at the higher applied load of 20 kN.

As expected from sensor calibration (Sect. 3.4), both sensors exhibited fluctuating measurements due to inherent noise. The potentiometer displayed low Standard Deviation (SD) values (8.0 µm to 28.8 µm), indicating consistent performance across all load steps. In contrast, the SD measurements for the IR sensor varied more significantly (36.2 µm to 211.7 µm), with its lower resolution limiting its accuracy in detecting small displacements (50 µm to 100 µm) compared to the potentiometer. The variations also substantially limited the achievable accuracy of the IR displacement sensor.

To further quantify the uncertainty, statistical analysis was conducted to compare the IR and potentiometer readings against the LVDT. The 95% confidence interval for the mean difference between the potentiometer and the LVDT was (−20.53 µm, 12.74 µm), with a mean difference of −3.89 µm. The p value from the paired t test was 0.621, indicating no statistically significant difference between the two sensors. These results substantiate the potentiometer's accuracy as its readings align closely with the control measurements. For the IR sensor, the 95% confidence interval

for the mean difference was (−172.92 µm, 55.32 µm), with a mean difference of −58.80 µm. The paired t test p value was 0.291, which, whilst not statistically significant, highlights a larger deviation compared to the potentiometer. This wider confidence interval underscores the IR sensor's greater variability and the resulting uncertainty in its displacement measurements in the static–cyclic load experiment.

5.2.2 Phase 2 – static–incremental load test

In the second phase of the load test, the RC-beam specimen underwent a static-incremental test load test, similar to the three-point bending test performed in Load Test Stage 1. Static loads were applied at the beam mid-span in 4-kN increments, up to a maximum of 52 kN, with each step applied over a minute and maintained for 2 min. Displacements were measured at the beam soffit during the test using the potentiometer contact sensor, IR non-contact sensor, and the LVDT control sensor, as shown in Fig. 23.

Mean displacements were calculated for each maintained load step by averaging all measured displacements during each maintaining period for all three sensors. The potentiometer showed MAE values ranging from 5.7 µm to 133.9 µm, with an overall average of 41.2 µm, closely matching the LVDT readings and demonstrating high accuracy. In contrast, the IR sensor had higher errors, with MAE values between 77.4 µm and 336.4 µm, and an average of 176.0 µm. It was observed that the error of the IR sensor gradually decreased at higher loads due to the reduced distance between the sensor and the beam.

The static–incremental test confirmed the potentiometer sensor's reliability, with low SD values (3.9 µm to 37.9 µm), indicating minimal variability in displacement readings and consistent performance. Statistical analysis further supported these findings, with a mean difference of −31.20 µm compared to the LVDT and a 95% confidence interval of (−73.50 µm, 11.10 µm). The paired t test resulted in a p value of 0.130, indicating no statistically significant difference between the potentiometer and the LVDT measurements. Note that the data selection was restricted between 0 and 36 kN due to excessive deformation from exceeding steel yield stress beyond this load range.

The IR sensor showed greater fluctuations in displacement readings, with SD values ranging between 31.4 µm and 141.5 µm, though a decreasing trend was observed at higher loads due to reduced noise at shorter IR detection distances. The statistical analysis revealed a mean difference of 66.49 µm, with a 95% confidence interval of (−91.58 µm, 224.56 µm). The paired t test resulted in a p value of 0.359, confirming no statistically significant difference between the

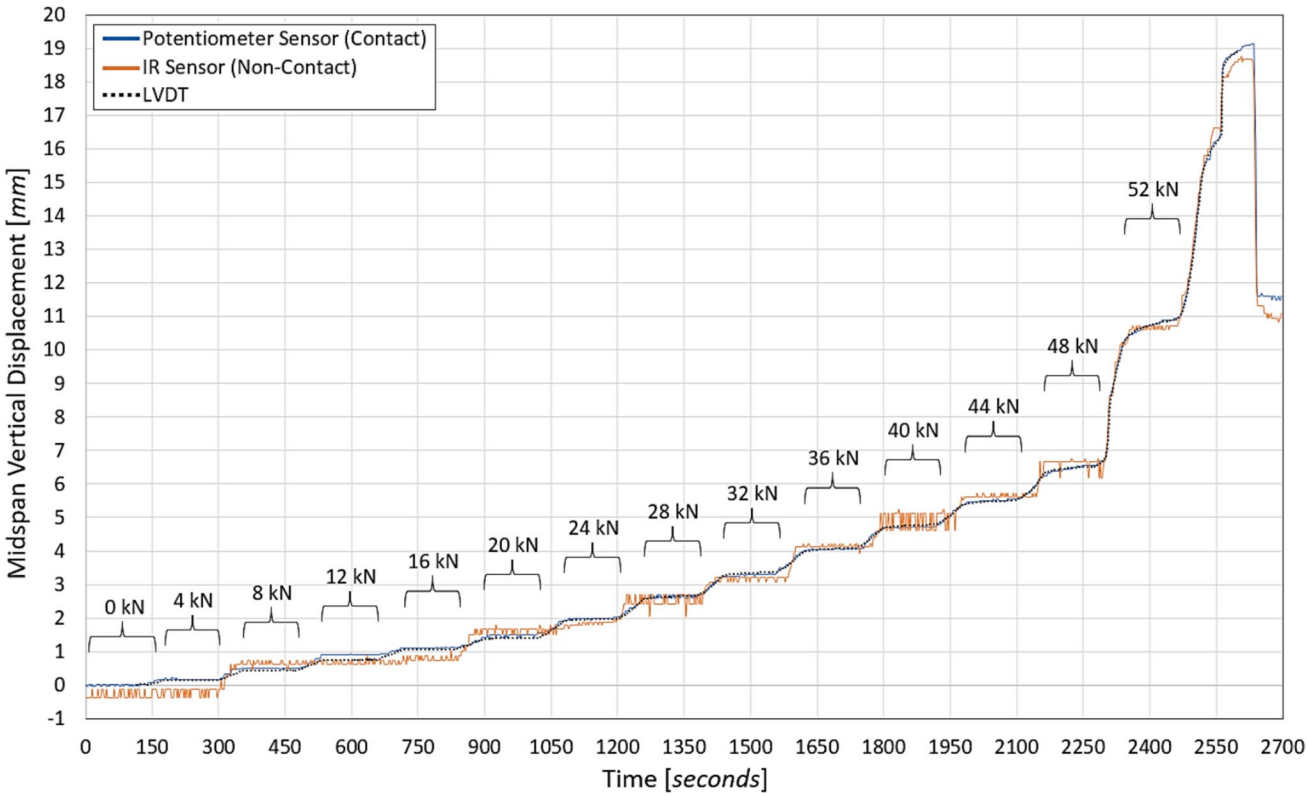

Fig. 23 Overall static–incremental test displacement results (Load Test Stage 2, Phase 2)

IR sensor and the LVDT measurements, though the IR sensor's higher variability and mean differences highlight its lower precision relative to the potentiometer.

5.2.3 Displacement sensor performance

The static–cyclic and incremental load experiments were intended to simulate the RC beam structural behaviour under typical day-to-day use and overloading conditions. The potentiometer contact sensor demonstrated excellent accuracy, with an average MAE of less than ± 50 µm, more precise than the preliminary estimated ± 80 µm during calibration. Statistical analysis from the static–incremental tests revealed a mean difference of −31.20 µm compared to the LVDT, with a 95% confidence interval of (−73.50 µm, 11.10 µm) and a p value of 0.130, indicating no statistically significant difference between the potentiometer and the LVDT measurements. The slight inaccuracy was partially attributed to hysteresis, which was initially determined to be 0.11% relative to its full extension. Throughout the experiment, the potentiometer exhibited minimal SD values, indicating high precision and measurement stability across different load levels.

Similarly, the IR non-contact sensor performed with an average MAE below ± 200 µm, better than the initially estimated ± 363 µm, which was determined during the sensor calibration stage. Statistical results from the static–incremental tests revealed a mean difference of 66.49 µm compared to the LVDT, with a 95% confidence interval of (−91.58 µm, 224.56 µm) and a p value of 0.359, confirming no statistically significant difference from the LVDT measurements. However, the IR sensor showed greater variability and less consistency due to its higher noise levels and lower resolution. Despite these limitations, the IR sensor was still capable of detecting submillimetre displacements, albeit with less precision than the potentiometer.

Overall, both proposed sensors demonstrated significant potential as low-cost, effective devices for measuring submillimetre displacements. The potentiometer, with its superior accuracy and reliability, is ideal for precise measurements, whilst the IR sensor remains a viable option in situations where close-proximity non-contact measurement is advantageous and higher error margins are tolerable. Both sensors can contribute to the practical and cost-effective implementation of a DT-integrated SHM framework.

5.2.4 Sensor IoT capability

The hardware system of the DT-based SHM framework was enhanced through the integration of the Arduino Nano 33 IoT wireless communication microcontroller. During the three-point bending experiments in Load Test Stage 2, the microcontroller established a wireless connexion to the internet. This connexion enabled real-time communication with the Arduino IoT Cloud, allowing for the immediate transmission and storage of displacement measurements on the platform. These data could be remotely accessed through a smartphone application (Fig. 24) or web browser downloaded for further review and processing.

The seamless integration of the Arduino with the DT-SHM framework streamlined the data transmission process, automating the flow of information from the physical structure to the digital model. This minimised the need for manual intervention, reduced potential errors, and accelerated post-processing procedures, ultimately improving the overall efficiency and responsiveness of the SHM process.

5.3 Post-processing result

Following the DT calibration and acquisition of sensor displacement data, a comprehensive post-processing procedure was performed to validate the DT-SHM framework. The DT, a numerical FE model simulating the RC beam's mechanical response, was integrated with real-time sensor data to estimate applied loads and predict crack formations and widths.

The GUI Window 3 of ReConTwin (Fig. 25) provided an intuitive and streamlined post-processing procedure. For each maintained load step during the static-incremental test test (Load Test Stage 2, Phase 2), displacement data retrieved from the potentiometer sensor were downloaded from the Arduino Cloud and locally saved for processing. The displacement files were imported into ReConTwin through the user interface for graphical review (Fig. 26a). Simultaneously, ReConTwin conducted an automated analysis of the imported displacement file, calculating the maximum and average beam deflection values during the recording period. Based on this information, the deflection value for each load step could be specified by the user in the prompt field. ReConTwin then estimated the imposed beam mid-span point load using a back-calculation procedure, interpolating the force from the force–displacement graph based on the specified displacement. The software allows the visualisation of this process alongside the DT force–displacement plot, as shown in Fig. 26b.

Using this workflow, the mid-span beam deflection for each applied 4 kN incremental load step was inserted into ReConTwin to estimate the corresponding imposed loads using the DT. The comparison between the experimental and DT-estimated loads is presented in Table 3. The final prediction was made at 52 kN, the maximum stable measurable load before failure.

The analysis of the imposed load data shows a consistent estimation by the DT model for applied loads between 8 and 32 kN, conservatively in favour of safety. The DT showed a peak underestimation of 5.18 kN at the 20 kN load step, with errors ranging from 0.57 kN to 3.89 kN. At higher

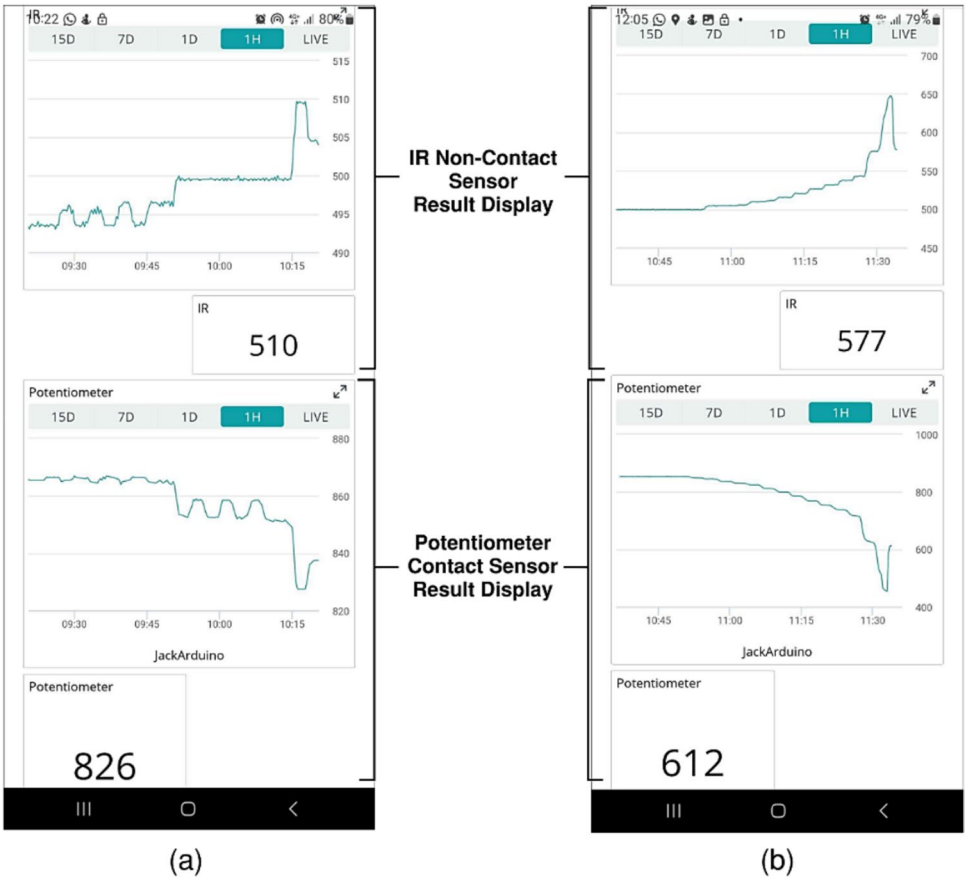

Fig. 24 Smartphone application Arduino IoT Cloud display of ADC digit result for the displacement sensors: **a** Static–cyclic test and **b** Static–incremental test

Fig. 25 ReConTwin: GUI Window 3, post-processing window

load levels exceeding the 36 kN load step, the DT model tended to overestimate the imposed loads, with errors ranging from 0.77 kN to 2.43 kN. This behaviour aligns with the force–displacement relationship depicted in Fig. 21b. Overall, the DT model achieved an average absolute error of 2.11 kN across all applied load step levels. This demonstrates that the DT model provides a highly accurate representation of the beam's mechanical response under varying load magnitudes.

In the final stage of the post-processing procedure, the displacement values obtained from the imported potentiometer data for each incremental load step were utilised to predict the crack formation of the RC-beam specimen. As part of the functionality of GUI Window 3, ReConTwin automatically executed *ReConAn FEA* to perform a displacement-controlled FE analysis. This analysis utilised both the specified basic property inputs and the iterating material property inputs of the DT model. Upon completion, *ReConAn Eye* was activated to provide a 3D graphical visualisation of the predicted crack patterns and animations of crack formation and beam deformation. The crack visualisation results were based on the proportioned applied displacement increment relative to the specified upper deflection limit used in the analysis. The comparison between the crack patterns predicted by *ReConAn FEA* and the actual crack patterns observed during the static–incremental load experiment in Phase 2 test of Load Test Stage 2 is illustrated in Fig. 27.

The predicted mid-span RC-beam soffit crack patterns generated by *ReConAn Eye*, although not identical to the actual observed patterns, demonstrated significant similarities in terms of general crack formation and spacing.

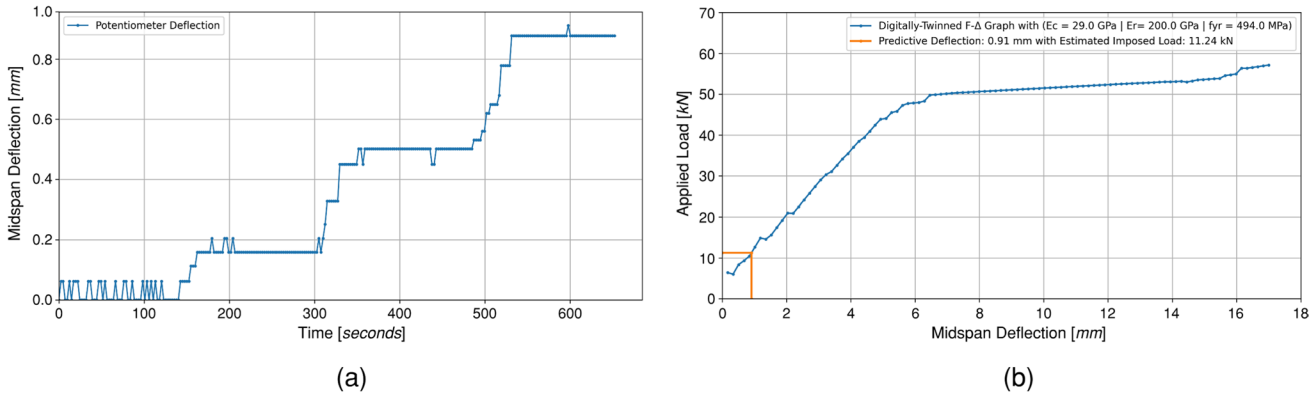

Fig. 26 ReConTwin, GUI Window 3 graphical plot: **a** Typical potentiometer displacement over the measured period from 4 to 12 kN and **b** Typical plot of back-calculated imposed point load on the DT force–displacement graph

Table 3 Comparison *of the experimental and DT-estimated imposed load*

Inserted Mid-span Deflection [mm]	Experimental Imposed Load [kN]	DT-Estimated Imposed Load [kN]	Absolute Error [kN]
0.142	4.00	5.37	1.38
0.443	8.00	7.44	0.57
0.757	12.00	9.84	2.16
1.067	16.00	13.27	2.73
1.398	20.00	14.83	5.18
1.957	24.00	20.11	3.89
2.636	28.00	24.98	3.01
3.34	32.00	30.79	1.20
4.055	34.00	36.77	0.77
4.758	40.00	42.43	2.43
5.47	44.00	46.08	2.07
6.46	48.00	49.78	1.78
10.69	52.00	51.78	0.22
		Average:	2.11

ReConAn FEA estimated an average crack spacing of 50 mm, which is slightly smaller than the observed average crack spacing of 79 mm. Overall, the potential damage to the beam was accurately predicted, showcasing the effectiveness of the *ReConAn FEA* software in predicting structural damage.

5.4 Beam damage diagnostic

As a final step in the DT-SHM process, the damage diagnostic was performed to assess the RC beam's structural condition and provide automated warnings for preventive actions if the beam was not performing within expected limits. During each incremental load step of the Load Test Stage 2 Phase 2 three-point bending test, two key performance indicators were monitored: mid-span deflection and estimated concrete crack width. This verification was implemented using GUI Window 4, where ReConTwin compared the mid-span deflection and crack width against the specified limits of a span-to-deflection ratio of 250 and a crack width limit of 0.3 mm, respectively, as shown in Fig. 28a. If either criterion exceeded these limits, ReConTwin generated a warning recommending preventive actions, as illustrated in Fig. 28b.

In the estimation of the concrete crack width, ReConTwin obtained the maximum strain value along the soffit of the FE beam corresponding to the specified incremental load step from the *ReConAn FEA* analysis output file. This strain value was multiplied by the FE hexahedral element mesh length (150 mm) to calculate the crack width. The reliability of the prediction is, therefore, highly dependent on the accuracy of the strain values determined by the DT model. The comparison of maximum beam soffit strains between the DT, as determined by *ReConAn FEA*, and the mean experimental results of Load Test Stage 1 under static 4-kN increments load steps is shown in Fig. 29.

The DT model slightly overestimated the strain between 8 and 12 kN, whilst it slightly underestimated the strain between 16 and 48 kN. Despite these deviations, the DT model closely matched experimental results, with an overall average absolute error of 281 με and an average relative error of 34.3%. Except for the 52-kN load step, where deformation caused a larger error, the DT demonstrated high accuracy in strain estimation, improving the reliability of predicted RC-beam soffit crack widths, especially for the total applied load below half of the ultimate load. These results underscore the DT model's effectiveness in approximating the beam's mechanical behaviour of the structural element, thereby ensuring the reliability of the damage diagnosis outcomes.

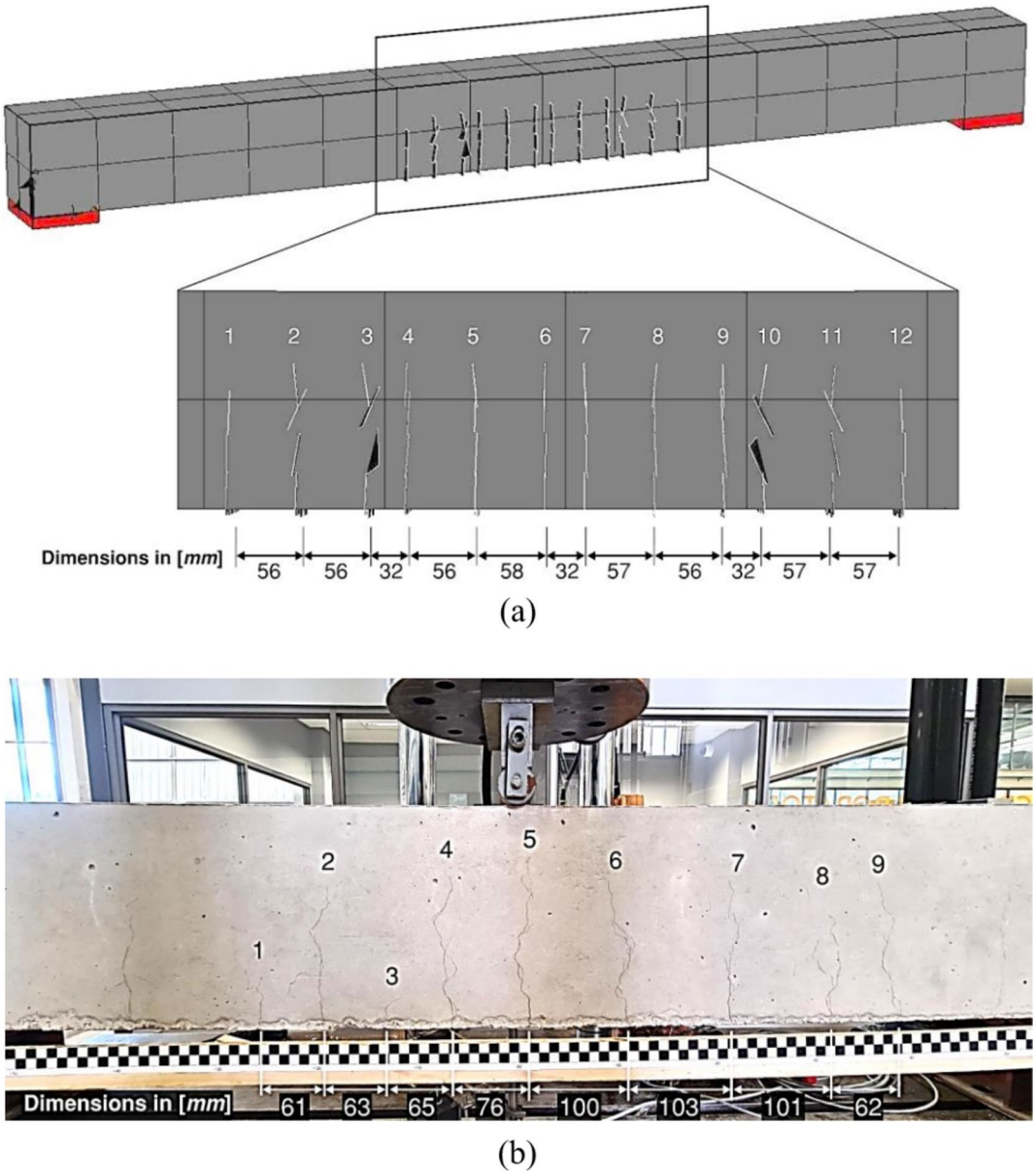

Fig. 27 Cracks along the soffit of the RC-beam specimen: **a** Predicted 3D crack formation in *ReConAn Eye* and **b** Experimental crack formations

6 Conclusions

This study introduced a potentiometer contact sensor and an IR non-contact sensor for structural displacement measurement, neither of which has been commonly used in past SHM systems. As sensor technology advances, these tools offer improved performance at lower costs, benefiting SHM systems for civil infrastructure. The potentiometer sensor demonstrated excellent accuracy, with a resolution under 50 µm and high measurement stability, making it suitable for precise measurements. The IR sensor, having a resolution varying between 100 µm to 300 µm with an accuracy below 200 µm, provided a viable option for non-contact measurements with slightly higher error margins. Both sensors proved to be reliable, low-cost solutions for submillimetre displacement monitoring, supporting the implementation of practical DT-integrated SHM frameworks.

The Arduino Nano 33 IoT microcontroller significantly enhanced the sensors' functionality in this experimental study's DT-based SHM system. During the three-point bending experiments, the Arduino enabled real-time data transmission from sensors to the IoT cloud, allowing remote data access and near real-time analysis. By leveraging the low-cost solution, this study demonstrated the feasibility of low-cost, wireless data transmission for SHM.

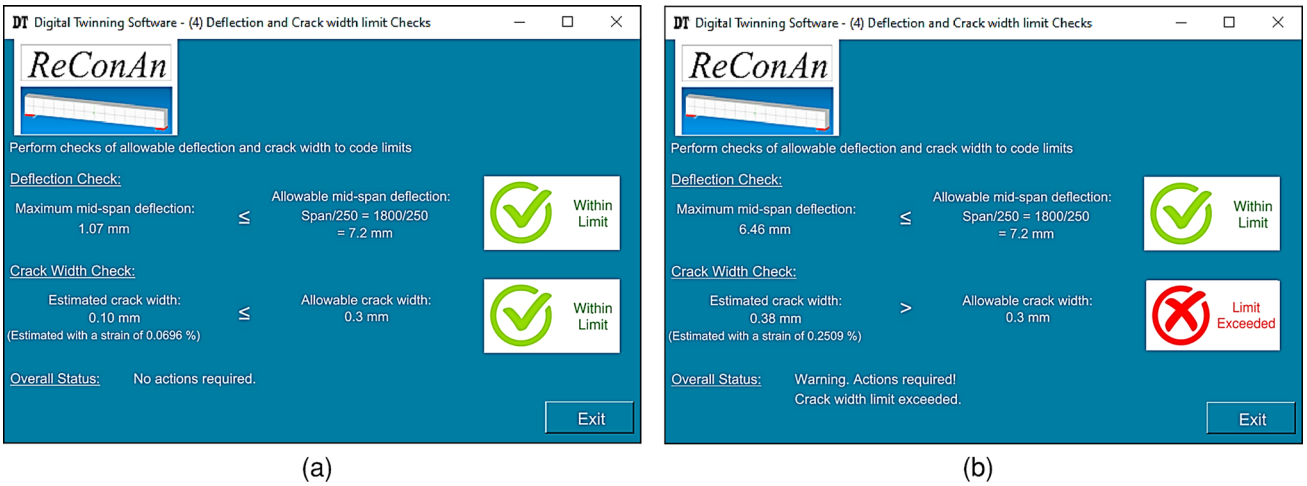

Fig. 28 ReConTwin, GUI Window 4, damage diagnostic procedure with deflection and crack width checks: **a** At applied load of 16 kN (within limit) and **b** At applied load of 48 kN (limit exceedance)

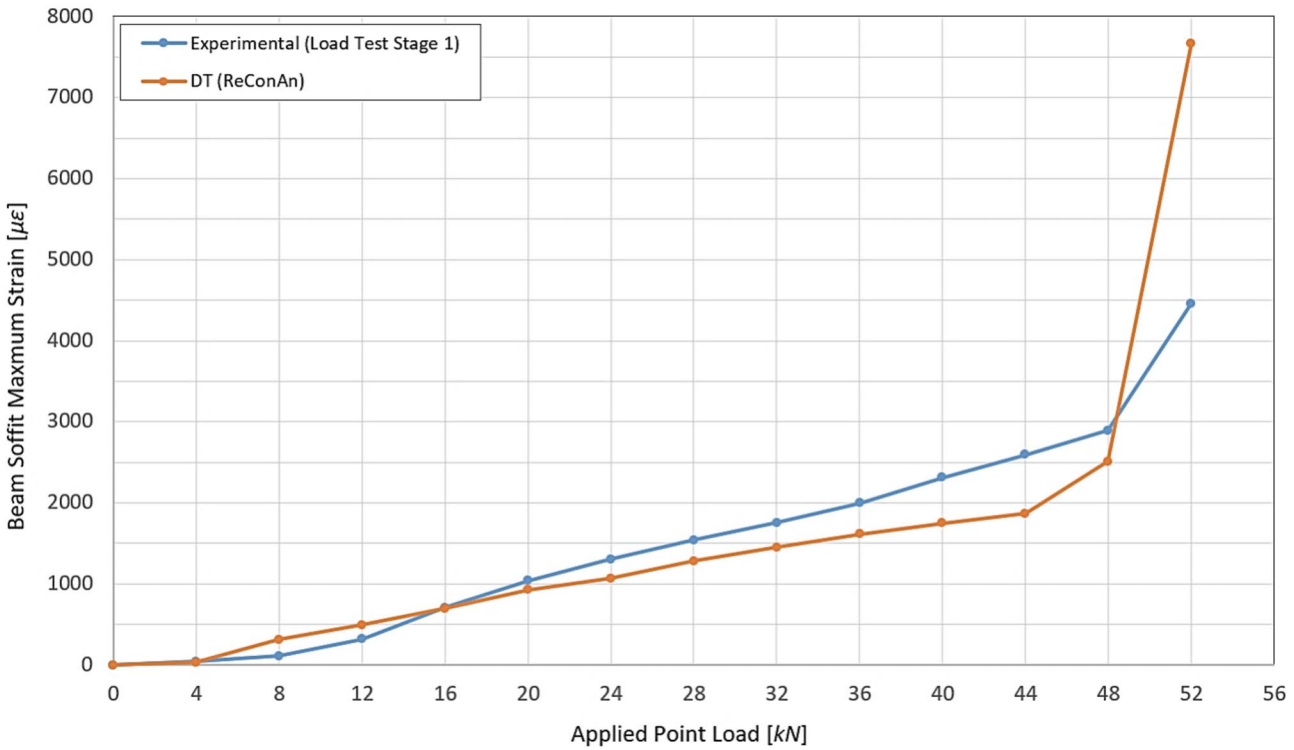

Fig. 29 Comparison of the experimental and DT-estimated maximum mid-span soffit strains

This research presents a practical, simplified approach for developing and processing a model-based numerical DT to predict the mechanical behaviour of an RC beam. Unlike traditional SHM systems, which are often expensive and complex, the proposed framework offers a roadmap towards a simpler, affordable, and accessible alternative for infrastructure asset monitoring. The principle of such system has been demonstrated in a controlled environment. Through an automated software pipeline, iterative structural analysis and material calibration were performed to simulate the beam's realistic bending stiffness and mechanical response. Developed in Python, the DT's calibration and post-processing were automated, whilst an intuitive GUI enhanced user interaction. In addition, the predicted mid-span RC-beam soffit crack patterns, generated by *ReConAn Eye*, showed significant similarities in general crack formation and spacing.

This functionality effectively provides users with further insights into the structural behaviour of the monitored RC member, demonstrating the effectiveness of both *ReConAn FEA* and ReConTwin in predicting structural damage not only at the superficial level but also internal damage at any 3D point within the RC domain. This predictive capability significantly enhanced the framework's damage diagnostics, enabling accurate identification of early-stage structural degradation and facilitating timely interventions. Furthermore, the FE nonlinear analysis using *ReConAn FEA* operates efficiently on standard computers, delivering reliable analysis results with a simpler data format compatible with various software applications and operating systems.

Although the DT development and calibration approaches undertaken in this study are specifically suited for straightforward SHM systems with simpler geometries, materials, and loading arrangements, their principles remain relevant for monitoring real-life civil infrastructures, which are often characterised by more complex geometries, material behaviours, environmental influences, physical imperfections, and varied load configurations.

In summary, this study confirms the feasibility of employing a DT-based SHM framework for civil infrastructure monitoring. By leveraging cost-effective IoT-enhanced microcontroller and relatively uncomplicated software solutions, this research demonstrates that the realisation of such systems is possible and can significantly enhance the efficiency and responsiveness of SHM processes.

Future work foresees the implementation of the proposed technology in real-scale structures such as important buildings and RC bridges. In addition, the ability of *ReConAn FEA* to perform nonlinear cyclic static [36] and dynamic analysis [37, 38] will be utilised in integrating the system with the ability to perform damage diagnostics through real-time data related to cyclic loading. Finally, the abilities to predict the mechanical response of RC structures through the use of *ReConAn FEA* extend to retrofitted structures as well [39], where the proposed DT-SHM framework with damage diagnostics can be implemented to rehabilitated and retrofitted structures.

Acknowledgements We gratefully acknowledge the funding provided by the China/South Africa project (Reference: CHIN2002255 06754, UID: 132787), and the support from the University of Pretoria's Department of Civil Engineering where the experiments were performed.

Funding Open access funding provided by University of Pretoria.

Data availability Some or all data, model, or codes that support the findings of this study are available from the corresponding author upon reasonable request.

Declarations

Conflict of interest The authors declare that they have no conflict of interest.

References

1. Agdas D, Rice JA, Martinez JR, Lasa IR (2015) Comparison of visual inspection and structural-health monitoring as bridge condition assessment methods. J Perform Constr Facil 30(3):04015049. https://doi.org/10.1061/(ASCE)CF.1943-5509.0000802
2. Graybeal BA, Phares BM, Rolander DD, Moore M, Washer G (2002) Visual inspection of highway bridges. J Nondestr Eval 21(3):67–83. https://doi.org/10.1023/A:1022508121821
3. Cawley P (2001) Non-Destructive Testing - Current Capabilities and Future Directions. Proceed Instit Mech Eng, Part L: J Mater: Design Appl 215(4):213–223. https://doi.org/10.1177/146442070121500403
4. Nagarajaiah S, Erazo K (2016) Structural monitoring and identification of civil infrastructure in the United States. Struct Monitor Main. https://doi.org/10.12989/smm.2016.3.1.051
5. Rehman SKU, Ibrahim Z, Memon SA, Jameel M (2015) Nondestructive test methods for concrete bridges: a review. Constr Build Mater 107(1):58–86. https://doi.org/10.1016/j.conbuildmat.2015.12.011
6. Errandonea I, Beltrán S, Arrizabalaga S (2020) Digital twin for maintenance: a literature review. Comput Indus. https://doi.org/10.1016/j.compind.2020.103316
7. Liu C, Zhang P, Xu X (2023) Literature review of digital twin technologies for civil infrastructure. J Infrastruct Intell Resilience. https://doi.org/10.1016/j.iintel.2023.100050
8. Mahmoodian M, Shahrivar F, Setunge S, Mazaheri S (2022) Development of Digital Twin for Intelligent Maintenance of Civil Infrastructure. Sustainability. https://doi.org/10.3390/su14148664
9. Armijo A, Zamora-Sánchez D (2024) Integration of Railway Bridge Structural Health Monitoring into the Internet of Things with a Digital Twin: A Case Study. Sensors 24(7):2115. https://doi.org/10.3390/s24072115
10. Bhatta S, Dang J (2024) Use of IoT for Structural Health Monitoring of Civil Engineering Structures: A State-of-the-Art Review. Urban Lifeline 2:17. https://doi.org/10.1007/s44285-024-00031-2
11. Chang H, Lin T (2019) Real-Time Structural Health Monitoring System Using Internet of Things and Cloud Computing. The 11th National Conference of Earthquake Engineering. Los Angeles, USA
12. Di Nuzzo F, Brunelli D, Polonelli T, Benini L (2021) Structural health monitoring system with narrowband IoT and MEMS sensors. IEEE Sensors J. https://doi.org/10.48550/arXiv.2104.13029
13. Ritto T, Rochinha F (2021) Digital twin, physics-based model, and machine learning applied to damage detection in structures.

Mech Syst Signal Process. https://doi.org/10.1016/j.ymssp.2021.107614
14. Shim CS, Dang NS, Lon S, Jeon CH (2019) Development of a bridge maintenance system for prestressed concrete bridges using 3d digital twin model. Struct Infrastruct Eng 15(10):1319–1332. https://doi.org/10.1080/15732479.2019.1620789
15. Yu S, Li D, Ou J (2022) Digital twin based structural hybrid monitoring and fatigue evaluation of orthotropic steel deck in cable stayed bridge. Struct Control Health Monitor. https://doi.org/10.1002/stc.2976
16. Kong X (2024) Monitoring time-varying changes of historic structures through photogrammetry-driven digital twinning. Int Arch Photogrammetry, Remote Sensing Spatial Informat Sci. https://doi.org/10.5194/isprs-archives-XLVIII-2-2024-181-2024
17. Hemdan EED, El-Shafai W, Sayed A (2023) Integrating digital twins with iot-based block chain: concept, architecture, challenges, and future scope. Wireless Pers Commun 131(1):2193–2216. https://doi.org/10.1007/s11277-023-10538-6
18. Chacón R, Casas JR, Ramonell C, Posada H, Stipanovic I, Škarić S (2023) Requirements and challenges for infusion of SHM systems within digital twin platforms. Struct Infrastruct Eng. https://doi.org/10.1080/15732479.2023.2225486
19. Interlab (2024) Solifos BRUsens V9. https://www.interlab.pl/en/product/solifos-brusens-v9.html. Accessed 13 March 2024
20. EFBElektronik (2024) Simplex Fiber Optic Patch Cable E2000. https://www.efb-elektronik.de/en/download/datasheet/?productNumber=O0834.10. Accessed 16 March 2024
21. fibrisTerre (2024) fTB 2505 Fiber Optic Sensing System for Distributed Strain and Temperature Monitoring. https://d3pcsg2wjq9izr.cloudfront.net/files/48898/download/348831/1-fibrisTerre_flyer.pdf. Accessed 16 March 2024
22. Variohm Eurosensor (2024) IPL Linear Position Sensor. https://www.farnell.com/datasheets/1833199.pdf. Accessed 17 March 2024
23. Sharp (2024) Distance Measuring Sensor Unit GP2Y0A41SK0F. https://global.sharp/products/device/lineup/data/pdf/datasheet/gp2y0a41sk_e.pdf. Accessed 23 March 2024
24. Arduino (2024) Arduino Nano 33 IoT Product Reference Manual. https://docs.arduino.cc/resources/datasheets/ABX00027-datasheet.pdf. Accessed 26 March 2024
25. Siemens (2023) Simcenter Femap Software. https://plm.sw.siemens.com/en-US/simcenter/mechanical-simulation/femap/. Accessed 25 April 2023
26. Mourlas C, Markou G (2020) ReConAn V2.00 Finite Element Analysis Software User's Manual. https://www.researchgate.net/publication/342361609_ReConAn_v200_Finite_Element_Analysis_Software_User's_Manual. Accessed 24 April 2023
27. Markou G (2011) Detailed Three-Dimensional Nonlinear Hybrid Simulation for the Analysis of Full Scale Reinforced Concrete Structures. PhD thesis, Institute of Structural Analysis and Seismic Research, National Technical University of Athens. https://doi.org/10.12681/eadd/24471
28. Markou G, Papadrakakis M (2013) Accurate and computationally efficient 3D finite element modeling of RC structures. Computers Concrete. https://doi.org/10.12989/cac.2013.12.4.243
29. Kotsovos MD, Pavlovic MN (1995) Structural Concrete. Finite element analysis for limit state design. Thomas Telford, London
30. Mourlas C, Markou G, Papadrakakis M (2017) 3D Nonlinear constitutive modeling for dynamic analysis of reinforced concrete structural members. Procedia Eng 199:729–734. https://doi.org/10.1016/j.proeng.2017.09.030
31. Roeloffze W, Markou G (2020) Finite element modelling of plain and reinforced concrete specimens with the kotsovos and pavlovic material model smeared crack approach and fine meshes. Int J Damage Mech. https://doi.org/10.1177/1056789520986601
32. Mourlas C, Papadrakakis M, Markou G (2016) Accurate and Efficient Modeling for the Cyclic Behavior of RC Structural Members. ECCOMAS Congress VII European Congress on Computational Methods in Applied Sciences and Engineering. Crete Island, Greece
33. Markou G (2013) Embedded reinforcement mesh generation method for large-scale RC simulations: case study. AHU J Eng App Sci 5(1):23–42. https://doi.org/10.1142/S021987621550019X
34. Visual Studio Code (2024) Learn to Code with Visual Studio Code. https://code.visualstudio.com/learn. Accessed 02 May 2024
35. Huang, J & Markou, G (2024) SMART Monitoring of Structures (Digital Twin, Live Data and Assessment). https://www.youtube.com/watch?v=SFZJZcM0xr4. Accessed 22 March 2024
36. Markou G, Mourlas C, Bark H, Papadrakakis M (2018) Simplified HYMOD non-linear simulations of a full-scale multistory retrofitted rc structure that undergoes multiple cyclic excitations – an infill rc wall retrofitting study. Eng Struct 176:892–916. https://doi.org/10.1016/j.engstruct.2018.08.002
37. Mourlas C, Markou G, Papadrakakis M (2019) Accurate and computationally efficient nonlinear static and dynamic analysis of reinforced concrete structures considering damage factors. Eng Struct 178:258–285. https://doi.org/10.1016/j.engstruct.2018.10.034
38. Mourlas C, Khabele N, Bark H, Karamitros D, Taddei F, Markou G, Papadrakakis M (2020) The effect of soil-structure interaction on nonlinear dynamic response of reinforced concrete structures. Int J Struct Stab Dyn 20(13):2041013. https://doi.org/10.1142/S0219455420410138
39. Markou G, Garcia R, Mourlas C, Guadagnini M, Pilakoutas K, Papadrakakis M (2021) A new damage factor for seismic assessment of deficient bare and FRP-retrofitted RC structures. Eng Struct. https://doi.org/10.1016/j.engstruct.2021.113152